November 2020

A Modelling Study for Smart Pigging Technique for Pipeline Leak Detection

Caitlyn Judith Thiberville
Louisiana State University and Agricultural and Mechanical College

A MODELLING STUDY FOR SMART PIGGING TECHNIQUE FOR PIPELINE LEAK DETECTION

A Thesis

Submitted to the Graduate Faculty of the
Louisiana State University and
Agricultural and Mechanical College
in partial fulfillment of the
requirements for the degree of
Master of Science

in

The Craft & Hawkins Department of Petroleum Engineering

by
Caitlyn Judith Thiberville
B.S., University of New Orleans, 2010
December 2020

ACKNOWLEDGEMENTS

I have many to thank for support throughout the years. To begin, my family has been and continues to be an endless source of encouragement. My advisor, Dr. Seung Ihl Kam, has guided me through research progress with patience and wisdom. My committee members, Dr. Paulo Waltrich and Dr. Wesley Williams, always left a door open for questions and generously gave material support in the laboratory. My graduate colleagues and friends including Dr. Renato Coutinho, who gave technical advice along with answers to my many questions; Dr. Mo Izadi, who welcomed me into the research group with the friendliest smile and with whom I've enjoyed many conversations on academics, culture, life; MaKuachukwu Mbaegbu who ventured with me into the world of Campus Life and Registered Student Organizations; my senior groups who toiled at PERTT Lab with me; and many others. I also must mention the PETE Professors, who teach with passion and determination to help every student see the light on many complex topics. Finally, I extend my deep appreciation to Louisiana Economic Development Assistantship (EDA) and State of Louisiana for financial support throughout this process; and Schlumberger for the generous donation of multiple software packages.

TABLE OF CONTENTS

LIST OF TABLES

LIST OF FIGURES

ABSTRACT

Although leak incidents continue, a pipeline remains the most reliable mode of transportation within the oil and gas industry. It becomes even more important today because the projection for new pipelines is expected to increase by 1 billion BOE through 2035. In addition, increasing number and length of subsea tiebacks face new challenges in term of data acquisition, monitoring, analysis, and remedial actions. Passive leak-detection methods commonly used in the industry have been successful with some limitations in that they often cannot detect small leaks and seeps. In addition to a thorough review of related topics, this study investigates how to create a framework for a smart pigging technique for pipeline leak detection, as an active leak detection method.

Numerical modeling of smart pigging for leak detection requires two crucial components: detailed mathematical descriptions for fluid-solid and solid-solid interactions around pig, and network modeling for the calculation of pressure and rate along the pipeline using iterative algorithms. The first step of this study is to build a numerical model that shows the motion of a pig along the pipeline with no leak, i.e., at a given injection rate, a pig first accelerates until it reaches its terminal velocity, beyond which the pig moves at a constant velocity. The second step is to construct a network model that consists of two pipeline segments (one upstream and the other downstream of leak location) through which the pig travels and at the junction of which fluid leak occurs. By putting these multiple mechanisms together and using resulting pressure signatures, this study presents a new method to predict the location and size of a leak present in pipeline.

INTRODUCTION

Leak detection is a well-defined subset of the pipeline industry, because of the economic and societal impacts of leak incidents. Pipeline leaks of hazardous liquid or gas can often cause irreparable damages to the environment, life, and public relations; therefore, prevention of the incidents is key. According to Henrie et al. (2016), the definition of a pipeline leak is "…the unintended escapement of commodity from pipelines due to a pipeline system integrity breach…", which can range from a small seep to a complete rupture. For oil and gas pipeline, the focus of this study, the breach typically occurs through the failure (either mechanically or chemically) of pipeline that is buried underground, spanning open space, or laid out in subsea area.

Brief History of Pipeline and Regulations

After first U.S. oil was struck in Titusville, PA in 1859, the main transportation of oil over land was by wagon. This system soon saw competition from continuous miles of oil pipeline, the first of which was a five-mile wrought iron line constructed in 1865 (Giddens, 1938). From this time, pipeline grew in length, standing as the main transmission path for crude oil. When blockages or constrictions in pipeline prevented fluid flow, operators turned to the inline cleaning tool so-called pig (pipeline inspection gauge).

This work was previously published as Thiberville, C., Wang, Y., Waltrich, P., Williams, W., & Kam, S. I. 2020. Modeling of Smart Pigging for Pipeline Leak Detection. SPE Production & Operations. DOI: 10.2118/198648-PA

As tools and technology to maintain and develop pipeline progressed, pipelines increased in continuous mileage to over 1,000 miles long in the 1920s. In the 1960s, pipeline pigs were further developed to include smart pigs (i.e., inspection pigs and devices that record information about the internal condition of a pipeline) whose features surpassed merely cleaning to include inline measurements, which enabled operators to address sections of pipe affected by buildup or corrosion (Tiratsoo 1992; PPSA 1995; Cordell and Vanzant 2003; Bai and Bai 2005). At this point in history, from the late 1960s and onward, the mileage of transportation pipeline in the U.S. grew significantly. In 2017, over 79,000 miles of crude oil pipeline, over 62,000 miles of liquid petroleum product pipeline, and over 2,500,000 miles of gas distribution, gathering, and transmission pipeline were recorded (U.S. Department of Transportation, 2018). Pipeline regulation and leak detection may seem an obvious necessity for such an intricate network transporting hazardous materials; however, the first U.S. pipeline federal regulation and establishment of the Office of Pipeline Safety did not occur until 1968, roughly 100 years after the first pipeline was laid. Since the Natural Gas Pipeline Safety Act of 1968 was adopted and amended in 1976 and 1979, several other congressional acts have passed including the Pipeline Safety Reauthorization Act of 1988, the Pipeline Safety Act of 1992, the Accountable Pipeline Safety and Partnership Act of 1996, and the Pipeline Safety Improvement Act of 2002 (Parker, 2004). Further updates, modifications and regulations were established with the Pipeline Inspection, Protection, Enforcement, and Safety Act of 2006 (Public Law 109-468), Pipeline Safety, Regulatory Certainty, and Job Creation Act of 2011 (Public Law 112-90), and Protecting Our Infrastructure of Pipelines and Enhancing Safety Act of 2016 (Public Law 114-183). Significantly, the result of legislation has been greater public awareness of pipeline safety and improved guidance on pipeline safety standards to establish “best practice” amongst industry

operators, particularly concerning pipeline leak detection, pipeline monitoring systems, and pipeline integrity management.

Legal descriptions classifying pipeline leaks may be found within the U.S. Code of Federal Regulations (CFR) Title 49. Existing CFR Title 49 for regulation of transportation systems was amended in 1994 by the 103rd Congress to include pipeline regulation under Subtitle VIII (Public Law 103-272). Since its passage, Subtitle VIII of Title 49 has been amended by the subsequent congressional acts mentioned previously and it covers topics from pipeline safety to fee scheduling. This fact is notable as all pipeline operator compliance in the U.S., including leak detection capabilities, is held to the standards outlined in Title 49. Details on how an incident is defined are available in the PHMSA Incident Report Criteria History document (PHMSA, 2018).

Guidance on pipeline safety and safe operation comes predominantly from recommendations by the standards body, American Petroleum Institute, or API. API Recommended Practices (API RP) 1130 and 1175 and API Technical Report (API TR) 1149 address topics of computational pipeline monitoring (CPM), leak detection program management, and the effect of pipeline variability and uncertainty on leak detection, respectively. API 1130 was written to give guidance on the design, implementation, testing, and operation of CPM systems. Herein, computational pipeline monitoring (CPM) is defined as "a term that was developed to refer to algorithmic monitoring tools that are used to enhance the abilities of a pipeline controller to recognize hydraulic anomalies that may be indicative of a pipeline leak or commodity release." CPM may be considered an internal, passive leak-detection method that utilizes single or multiple pipeline parameter measurements, such as pressure, temperature, viscosity, density, flowrate, product sonic velocity, or product interface location along with computation by the controller or electronic system to detect a leak. Although CPM is a primary component in most leak-detection

systems, it often plays a role as part of a team of systems encompassing the pipeline operator's Leak Detection Program (LDP), as shown by API RP 1175.

Evolution of Leak Detection and Pigging Technique

As pipeline networks grew after World War II and governmental agencies developed to ensure public and environmental safety surrounding hazardous fluid transport, pipeline leak detection and testing became a field of its own. Until acoustic and electric current pigs were developed, the dominant method of leak detection was hydrostatic pressure testing whereby a line must be taken out of service for testing. Although still in use today, this process is time consuming and inefficient, particularly in light of the extensive mileage in play currently. In the late 1960s and throughout the 1970s, acoustic pigs began gaining traction as a reliable in-line leak detection technique (Riemsdijk and Bosselaar, 1967; Fluornoy and Schroeder, 1978).

In conjunction with pigging techniques, pipeline simulation gained steam in the 1970s and was subsequently used for development of leak detection programs. Using computer simulation, Chan (1980) found the parameters most sensitive as leak detection "Sensing Parameters" to be rate of pressure drop and rate of flow. Early publications of studies employing similar computer-based simulations blossomed throughout the 1980s. The concept of Real-Time monitoring for leak detection, whereby pressure and temperature data is gathered in real-time and compared to a computer based model of the pipeline system, using standard supervisory control and data acquisition (SCADA) information was presented by Dupont et al. (1980) and proven for gas line applications by Burson et al. (1986). After that, Bednorz and Pringle (1998) employed simulation methods to study the effects of instrumentation spacing on real-time leak detection. Stafford and Williams (1996) and Wuori et al. (2000), however, concluded that no "new breakthroughs" had

been made in the early 1990s, with the exception of fiscal improvements to fiber optic technology, and the focus should be made on leak prevention and rapid detection.

The ADEC (2012) report noted an impressive improvement to existing computational leak detection, that was, the use of statistical analysis and learned behavior to determine a leak condition in combination with real time transient modelling (Geiger and Werner 2003; Salmatanis et al. 2015). In addition, the smart-pig technology presented by Elliott et al. (2008) refined the capabilities of acoustic detection to a small diameter pig able to flow freely in the product line.

Several other studies that may contribute to development of an omniscient pig assisted leak-detection methodology include Shannon et al. (1985), Tolmasquim and Nieckele (2008), Mirshamsi and Rafeeyan (2012), and Lima et al. (2017). Tolmasquim and Nieckele (2008) developed numerical coding using a finite difference scheme to solve the transient pressure and velocity fields imposed on a pipeline when oil is displaced by a sealing pig. The combined equations of continuity and momentum for fluid flow along with an equation coupling the fluid flow with pig motion, first developed by Azevedo et al (1996), were employed to model the mechanics of pig motion, then discretized to solve the time dependencies. In addition, they successfully implemented a proportional-integral-derivative (PID) controller to maintain a set threshold of desired pipeline pressure or pig velocity. With two test cases, the potential of the controller method for implementation in the field was proven for efficient pigging operations.

Years later, Mirshamsi and Rafeeyan (2012) used quantitative feedback theory (QFT) to show that pig velocity can be kept constant, as desired, during runs to ensure measurement quality and accuracy. A majority of inline inspection tools (ILI) or smart pigs are used to evaluate the reduction in metal thickness due to corrosion. Magnetic flux leakage technology is typically employed for this measurement, and it is negatively affected by excessive pig speed and lift-off

from the pipe wall. This type of velocity control measure may prove useful if pig assisted leak detection is used in combination with pressure transducer-fitted leak detection pigs, such as the one created by Camerini et al. (2004). A study by Lima et al. (2017) proved experimentally that a parameter vital to pig assisted leak detection, that is, pig velocity, could be determined by commonly monitored parameters. Their study sought to determine pig velocity using pipeline pressure transducers and supervisory data. With direct measurement of velocity (Ramsden 2006), which correlates measured voltage to velocity, mounted on the pig, they were able to confirm their velocity calculations using transducers and Supervisory Control and Data Acquisition (SCADA) information. Chatzigeorgiu et al. (2013) recently showed the pressure signature of a leak in water pipeline that can be detected by a robotic device or smart pig without interruption to flow. The device is able to detect even small leaks of a minimum 1 gal/min to within 1-foot location accuracy by exploiting the suction force of commodity release on a flexible skirt that runs the diameter of the pipeline. In their laboratory- and field-scale testing of a leak detection pig, Camerini et al. (2004) found that the leak location could be estimated by measuring the differential pressure across the pig.

The current trends and obstacles in the evolution of leak detection are shown by the 2016 U.S. Pipeline and Hazardous Materials Safety Administration's (PHMSA) peer review report. The report shows an analysis of projects on a scale of Ineffective to Very Effective and, as reported, the topics on leak detection include studies to optimize existing leak detection technologies, pipeline survey using side-scan lasers for small natural gas leaks, and differential absorption lidar (DIAL) for aerial detection of methane leaks (Emery et al., 2016). In 2018, further update on the project listed notable strides in leak detection technology to include a small diameter, free flowing internal smart-pig leak detection based on acoustic sensing, further development in aerial survey

for pipeline leak detection, and the use of spectroscopy to detect vapors from liquids pipeline leaks (Secor 2018).

Modelling Pig Motion

Literature regarding the mechanistic modeling and experimental study of pig movement in pipeline is prolific. In reviewing available literature, researchers began studying the motion of both spheres and capsules (i.e. cylinders) in liquid and gas pipe in the late 1950s and early 1960s (Govier and Aziz 1972; McDonald and Baker 1964). Operators began using spheres for liquids removal in 1958 and later for batching or product separation, while discussion of cylindrical capsule use, in contrast, began as a means to efficiently transport solids in pipe (Govier and Aziz 1972). Common parameters determined mechanistically and monitored experimentally in these early studies include stiction pressure necessary to move a stationary pig (or overcome static friction), the driving pressure necessary to keep a pig in motion once a balance of forces has been reached, the effect of pig dimensions, and the pig velocity, to name a few.

Pig motion through a pipeline is affected by characteristics of the pig, the driving fluid, and the pipeline. Hara et al. (1978) reported experimental results of deploying a spherical pig in 4-in, 1,300-m horizontal test-line while flowing fluids of varying density and viscosity, namely water, kerosene, and gasoline. Azevedo et al. (1996) modeled the mechanisms of a bypass pig (i.e., a pig with multiple bypassing holes) moving in a line similar to that of Hara et al. (1978). Modeling a pig in a 4-in, 1,300-m horizontal line, the group found the pressure drop across the pig could be predicted by mechanistic modeling of the fluid flow through the bypass holes and across an idealized gap between the pig outer diameter and the pipe inner diameter.

MOTIVATION AND OBJECTIVES

Even with continued evolution in the field of leak detection and extensive guidance, pipeline operators have not been able to maintain a consistent incident decline trend. Henrie et al. (2016) show spills have declined since 2002; however, since 2007 the decline trend has flattened (Fig. 1) and indicates pipeline leaks persist inevitably. Although detection systems are in place, both Shaw et al. (2012) and Henrie et al. (2016) noted that a majority of leaks reported to PHMSA are more likely to be detected by direct visual observation. This statement implies the predominant leak-detection method has not changed from visual observation since the previous comprehensive U.S. leak detection study published in 1982 (Mastandrea, 1982). Perhaps these statistics have improved since the API TR 1149 (2015) recommendations were published, but a comprehensive leak detection study is yet to be complete.

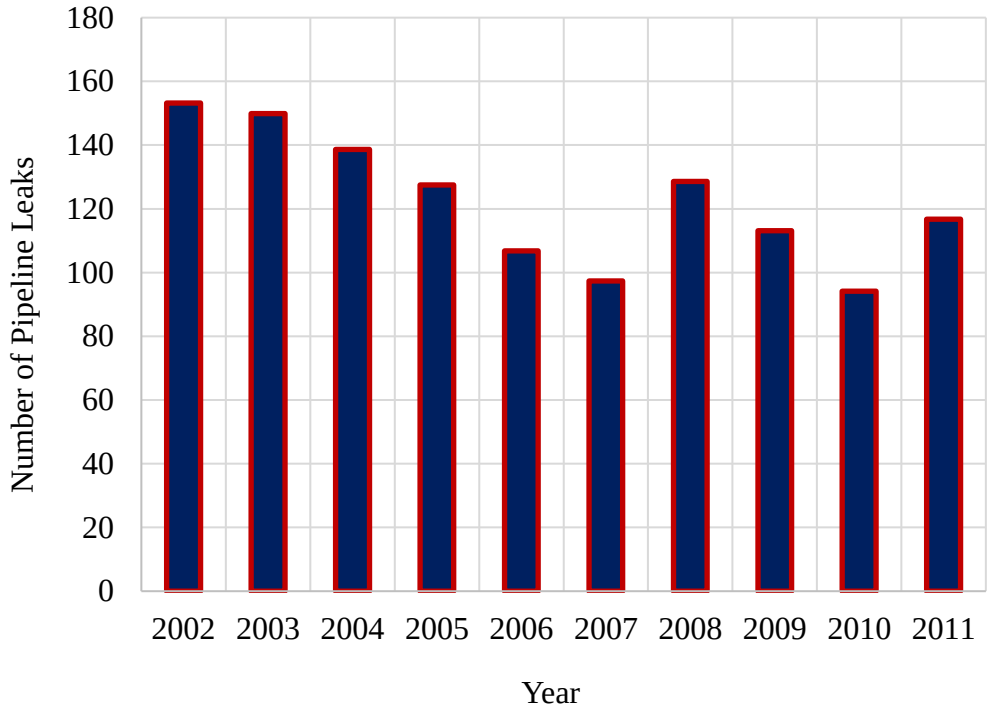

Figure 1. U.S. Pipeline and Hazardous Materials Safety Administration right-of-way reported leaks (*Source*: modified from Henrie et al. (2016)).

Prompted by experimental and mechanistic studies on leak detection (such as Scott et al. (1999), Smith and Griffin (2001), Gajbhiye and Kam (2008), and Kam (2009), which use a passive approach to leak detection by employing commonly monitored parameters such as pressure and flowrate), Thiberville et al. (2017) extended the concepts of previous mechanistic models to a Gulf of Mexico (GOM) case study using numerical simulations. These modeling and simulation studies evaluate a wide range of multiphase flow scenarios in the pipeline in terms of the changes in pressures and/or flow rates as leak detection indicators at various values of backpressure, pipe diameter, inlet gas-oil ratio, water depth, water cut, riser presence, inclination angle, and boundary conditions, among many. The use of contour plots, presenting the variations in terms of pressure and total flowrate (ΔP and Δq_t), is shown to be a useful means of monitoring possible pipeline leak and back-calculating leak characteristics such as leak position (x_{leak}) and opening size (d_{leak}). This then prompted the current study that aims to combine the use of commonly monitored parameters with the smart pigging, or to marry the passive and active approaches of pipeline leak detection.

Therefore, this study for the first time presents a mathematical framework for leak-detection technique combined with smart pigging. The results are presented in terms of unique pressure signatures which are related to the location and size of pipeline leak.

In addition, this study also demonstrates how different pieces of knowledge can be implemented together for leak-detection purpose, including (i) the physics of fluid flow through and around a bypass pig in a horizontal pipeline, (ii) the relationships among fluid velocity (or flowrate), pig velocity, and pressure drop across the pig, and (iii) formulation of leak-detection problem using network model and smart pigging.

METHODOLOGY

In order to describe pig motion within the pipeline, this study employs a hydrodynamic model for a bypass-type pig developed by Azevedo et al. (1996) as shown in Fig. 2, where the pig (with length L_{pig} and outer radius R_{pig}) is moving at the velocity of V_{pig} in a pipe (with inner radius R_{pipe} (or inner diameter d_{pipe})) filled with incompressible aqueous phase (i.e., water, with density of ρ_w and viscosity of μ_w). The constant inlet water flow rate of q_w across the pipe cross-sectional area (πR_{pipe}^2) splits into (i) the flow rate through the gap between pipe inner surface and pig outer surface (q_{wgap}) and (ii) the flow rate through the hole within the pig (q_{whole}). Note that the gap (δ) is given by (R_{pipe}-R_{pig}), while the hole has hole radius R_{hole} and length L_{hole} (that is, the same as L_{pig}). Over the pig length of L_{pig}, the pressure drop across the pig is given by ΔP_{pig} that is no other than the difference between the pressure at the upstream of the pig (P_{upp}) and the pressure at the downstream of the pig (P_{dnp}). Also note that the horizontal pipeline extends from the inlet ($x = 0$ where $P = P_{in}$) to the outlet ($x = L_{pipe}$ where $P = P_{out}$) with pig upstream and downstream located at $x = x_{pig}$ and $x = x_{pig} + L_{pig}$, meaning that $P = P_{upp}$ at $x = x_{pig}$ and $P = P_{dnp}$ at $x = x_{pig} + L_{pig}$. Incompressible flow allows the water flow rate of q_w maintained along the pipeline, including the inlet ($q_w = q_{win}$) and outlet ($q_w = q_{wout}$). Note that, by saying smart pigging technique, this study assumes the pressure values at the upstream and downstream ends of the pig (P_{upp} and P_{dnp}) are monitored with time—and available.

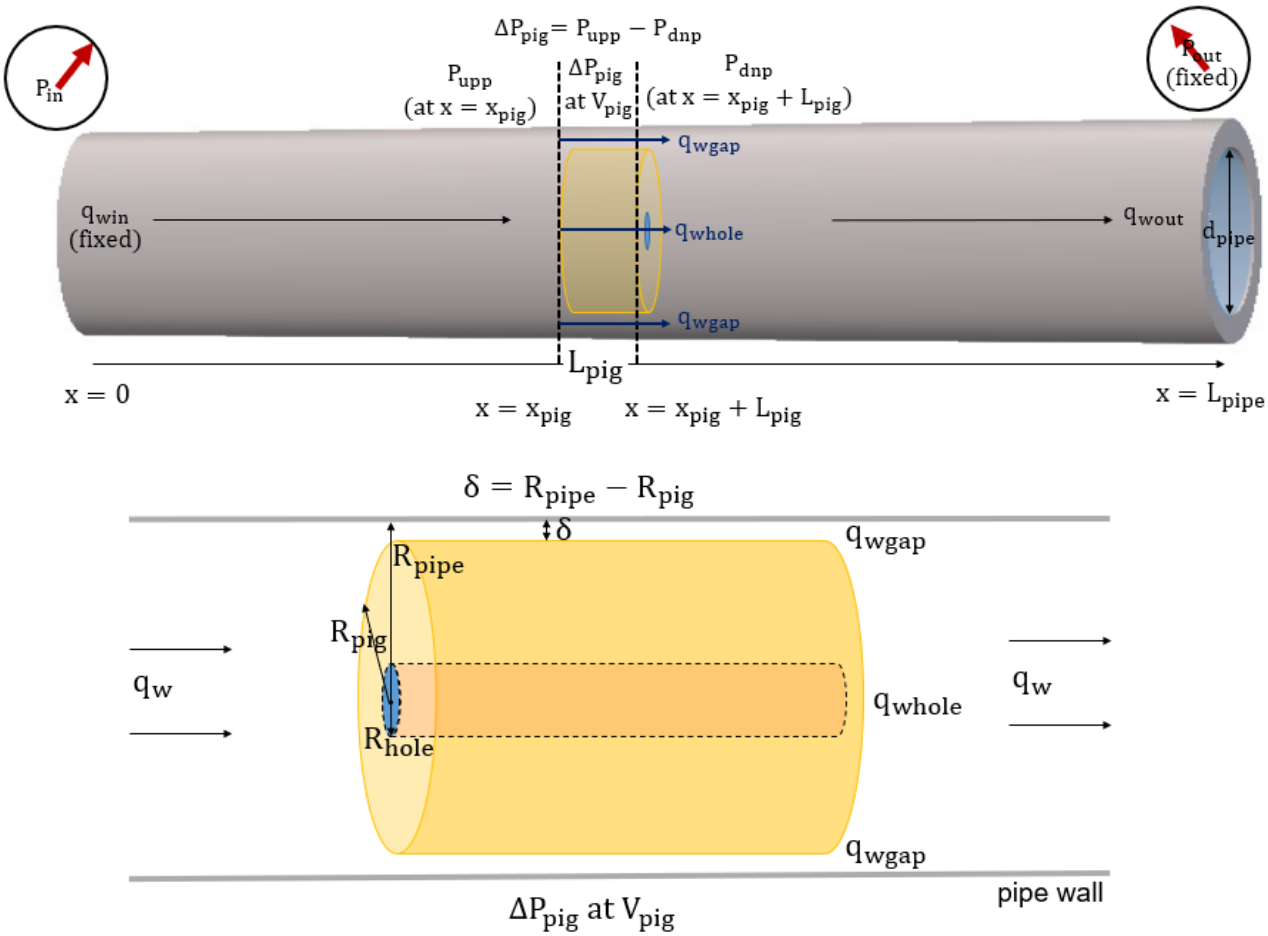

Figure 2. Schematic representation of model parameters describing a pig in motion in horizontal pipeline.

The equations in Azevedo et al. (1996) can then be summarized as follows:

$$q_{wgap} = 2\pi R_{pipe}\left(\frac{\delta^3}{12\mu_w}\frac{\Delta P_{pig}}{L_{pig}} - \frac{\delta}{2}V_{pig}\right) \quad (1)$$

$$q_{whole} = \frac{\pi\sqrt{2}(2R_{hole})^2}{4}\sqrt{\frac{\Delta P_{pig}/\rho_w}{k+fL_{hole}/2R_{hole}}} \quad (2)$$

where, k and f represent the entrance/exit effect due to the hole in the pig and the friction factor through the hole, respectively. Note that the flow through the gap mimics the one for a slit geometry, and these equations deal with laminar flow that typically occurs when the pig is in motion.

At the injection rate of q_w, the bypassing flow rate around and across the pig (q_{wbp}) is defined as

$$q_{wbp} = q_{wgap} + q_{whole} \tag{3}$$

which makes

$$q_{wbp} = q_{win} - \pi R_{pig}^2 V_{pig} \tag{4}$$

for incompressible flow. Fluid mechanics defines shear force (F_s) created by the fluid flowing across the pig and through the gap and frictional force (F_{fr}) between the pig and pipe wall as follows:

$$F_s = 2\pi R_{pipe} L_{pig} \left(\frac{1}{2} \frac{\Delta P_{pig}}{L_{pig}} \delta - \mu_w \frac{V_{pig}}{8} \right) \tag{5}$$

$$F_{fr} = F_s + \pi R_{pipe}^2 \Delta P_{pig} \tag{6}$$

Because Azevedo et al. (1996) show that the contact forces are not coupled to hydrodynamic forces with the exception of large oversize pig cups, this study derives equations

below to relate the pressure drop across the pig (ΔP_{pig}), water flow rate (q_w, q_{win} and q_{wout}), and pig velocity (V_{pig}).

$$q_{whole} = \frac{\pi\sqrt{2}(2R_{hole})^2}{4}\left(\frac{\Delta P_{pig}/\rho_w}{k+fL_{hole}/2R_{hole}}\right)^{\frac{1}{2}} \tag{7}$$

$$q_{wgap} = 2\pi R_{pipe}\left(\frac{\delta^3}{12\mu_w}\frac{\Delta P_{pig}}{L_{gap}} - \frac{\delta}{2}V_{pig}\right) \tag{8}$$

$$q_{wgap} + q_{whole} = q_{win} - \pi R_{pig}^2 V_{pig} \tag{9}$$

Once the equations are solved for ΔP_{pig}, it can be shown as follows:

$$B^2\Delta P_{pig}^2 + (-2AB - C)\Delta P_{pig} + A^2 = 0 \tag{10}$$

where

$$A = q_{win} - \pi R_{pipe}^2 V_{pig} + \pi R_{pipe}\delta V_{pig} \tag{11}$$

$$B = \frac{\pi R_{pipe}\delta^3}{6\mu_w L_{gap}} \tag{12}$$

$$C = \left(\pi\sqrt{2}(2R_{hole})^2\right)^2\left(\frac{1}{\rho_w(k+fL_{hole}/2R_{hole})}\right) \tag{13}$$

Concurrently, the pressure gradient within the aqueous phase where no pig is present ($0 < x < x_{pig}$, or $x_{pig} + L_{pig} < x < L_{pipe}$) can be calculated by the Darcy-Weisbach frictional pressure loss equation as detailed by Brill and Mukherjee (1999), i.e.,

$$\left(\frac{dP}{dx}\right)_f = \left(\frac{f\rho_w\left(q_{win}/\pi R_{pipe}^2\right)^2}{4R_{pipe}}\right) \tag{14}$$

where, the Moody friction factor (f) is obtained from

$$f = 64/Re \tag{15}$$

if laminar flow or

$$\frac{1}{\sqrt{f}} = -2\log_{10}\left(\frac{\epsilon/(2R_{pipe})}{3.7} + \frac{2.51}{Re\sqrt{f}}\right) \tag{16}$$

with the absolute roughness ϵ, if turbulent. The Reynolds number (Re) is defined as

$$Re = \frac{\rho_w\left(q_{win}/\pi R_{pipe}^2\right)2R_{pipe}}{\mu_w} \tag{17}$$

Next, suppose a leak is imparted on the pipeline at a given longitudinal leak location ($x = x_{leak}$) with a circular leak-opening size of diameter d_{leak} (or radius R_{leak}), leading to a leak flow rate of q_{leak}. As shown in Fig. 3, the solution scheme in such a scenario depends on whether the pig in motion is located upstream or downstream from the leak.

When the pig is located upstream of the leak, the inlet pressure (P_{in}) is a result of the following 4 components:

(i) the pressure drop downstream of the leak (i.e., $x = x_{leak}$ to L_{pipe}), with a flowrate equal to $q_{wout} = q_{win} - q_{leak}$,

(ii) the pressure drop of the pipe upstream of the leak but downstream of pig (i.e., $x = (x_{pig} + L_{pig})$ to x_{leak}) with a flowrate equal to q_{win},

(iii) the pressure drop across the pig (ΔP_{pig}) (i.e., $x = x_{pig}$ to $(x_{pig} + L_{pig})$), and

(iv) the pressure drop upstream of the pig (i.e., $x = 0$ to x_{pig}) with a flowrate equal to q_{win}.

If the outlet pressure (P_{out}) is given, this allows an equation for P_{in} to be written as follows:

$$P_{in} = P_{out} + \left(L_{pipe} - x_{leak}\right)\left(\frac{dP}{dx}\right)_{f,q_{win}-q_{leak}} + \left(x_{leak} - (x_{pig} + L_{pig})\right)\left(\frac{dP}{dx}\right)_{f,q_{win}} + \Delta P_{pig} + x_{pig}\left(\frac{dP}{dx}\right)_{f,q_{win}} \quad (18)$$

If the pressure at the junction (i.e., at the leak) is given by P_{junc}, Eq. (18) becomes

$$P_{in} = P_{junc} + \left(x_{leak} - (x_{pig} + L_{pig})\right)\left(\frac{dP}{dx}\right)_{f,q_{win}} + \Delta P_{pig} + x_{pig}\left(\frac{dP}{dx}\right)_{f,q_{win}} \quad (19)$$

where

$$P_{junc} = P_{out} + \left(L_{pipe} - x_{leak}\right)\left(\frac{dP}{dx}\right)_{f,q_{win}-q_{leak}} \tag{20}$$

Or, equivalently,

$$P_{junc} = P_{out} + \left(\frac{f\rho_w\left(L_{pipe}-x_{leak}\right)}{4R_{pipe}\left(\pi R_{pipe}^2\right)^2}\right) \times \left(q_{win} - q_{leak}\right)^2 \tag{21}$$

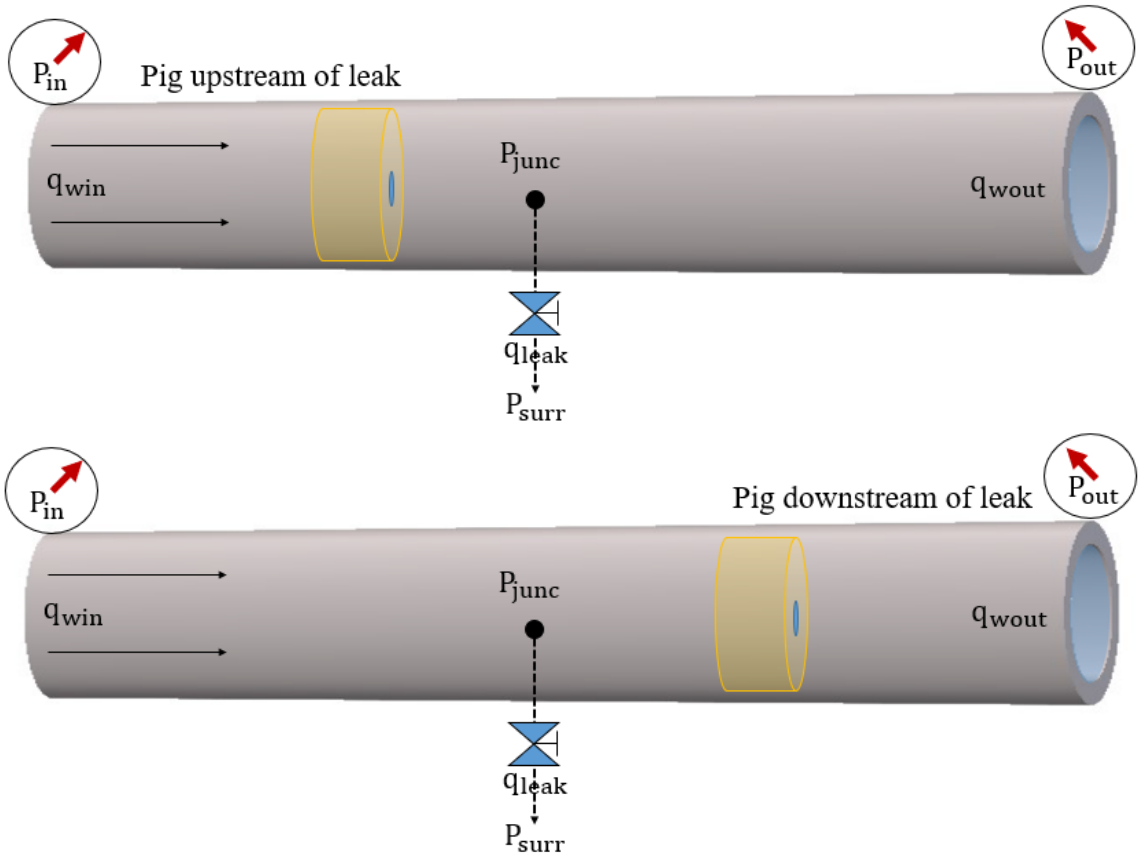

Figure 3. Schematic drawing of pig location ($x = x_{pig}$) with respect to the leak ($x = x_{leak}$) with opening size of d_{leak}.

Note that P_{junc} can also be determined from the surrounding pressure (P_{surr}) outside the leak and the leaking flow rate (q_{leak}), i.e.,

$$P_{junc} = P_{surr} + \left(\frac{\rho_w}{2\left(\pi d_{leak}^2/4\right)^2 c_{leak}^2}\right) \times q_{leak}^2 \tag{22}$$

where c_{leak} is a leak coefficient which is constant 0.85 for water according to API 14B (2005) (PIPESIM 2013). The concept of a network model forces these two junction pressure values in Eqs. (21) and (22) to be identical. This allows the unknown q_{leak} to be determined by iteration.

A similar approach can be applied when the pig is located downstream of the leak, i.e.,

$$P_{in} = P_{out} + \left(L_{pipe} - (x_{pig} + L_{pig})\right)\left(\frac{dP}{dx}\right)_{f,q_{win}-q_{leak}} + \Delta P_{pig} + \left(x_{pig} - x_{leak}\right)\left(\frac{dP}{dx}\right)_{f,q_{win}-q_{leak}} + x_{leak}\left(\frac{dP}{dx}\right)_{f,q_{win}} \tag{23}$$

If P_{junc} is used, Eq. (23) becomes

$$P_{in} = P_{junc} + x_{leak}\left(\frac{dP}{dx}\right)_{f,q_{win}} \tag{24}$$

where

$$P_{junc} = P_{out} + \left(L_{pipe} - (x_{pig} + L_{pig})\right)\left(\frac{dP}{dx}\right)_{f,q_{win}-q_{leak}} + \Delta P_{pig} + \left(x_{pig} - x_{leak}\right)\left(\frac{dP}{dx}\right)_{f,q_{win}-q_{leak}} \tag{25}$$

Similarly, Eq. (25) can be used together with Eq. (22) to determine P_{junc} and q_{leak} by iteration. Note that the iteration when the pig is located downstream of the leak is more complicated, because the term ΔP_{pig} is also a function of flowrate of (q_{win} - q_{leak}) where q_{leak} is required to be calculated by iteration.

Sometimes, it is convenient to use the pressure drop across the leak (ΔP_{leak}) for analysis as follows:

$$\Delta P_{leak} = P_{junc} - P_{surr} = \frac{\rho_w \times \left({}^{4\, q_{leak}}/_{\pi d_{leak}^2} \right)^2}{2} \times \frac{1}{c_{leak}^2} \tag{26}$$

which can also be written as

$$d_{leak} = 2 \left(\frac{q_{leak}}{\pi c_{leak} \sqrt{\frac{2(\Delta P_{leak})}{\rho_w}}} \right)^{1/2} \tag{27}$$

if leak opening size (d_{leak}) needs to be calculated.

At this stage, this study assumes one-dimensional horizontal flow, incompressible single-phase flow, a particular type of pig, and clean and uniform pipe surface. Some of these assumptions can be relaxed in the future, as briefly discussed in the later section (for example, effects of multiphase flow and compressible phases). Although the equations are developed for a bypass-type pig, other types of pig can also be used in the same manner as long as the relationships among q_w, V_{pig}, and ΔP_{pig} are provided.

RESULTS

As a base-case scenario, this study considers a pipeline with no leak first. Input parameters for this base-case scenario are taken from actual experiments (Azevedo et al. 1996) and summarized in Table 1, where the pipeline has 4-inch (0.0486-m) ID and 4,265-ft (1300-m) horizontal length with a bypass-type pig. The bypass pig is chosen because of its popularity in industry to avoid excessive sticking and blockage. The pig terminal velocity (V_{pigT}) of 1.14 m/s (or 3.74 ft/s), borrowed from Azevedo et al. (1996), is common in field-scale operations (Cordell and Vanzant 2003).

Fig. 4 shows a typical pig motion when a pig is launched: (i) the pig accelerates (at the rate of a_{pig}) and its velocity (V_{pig}) increases from $V_{pig} = 0$ (at $t = 0$) to $V_{pig} = V_{pigT}$ (at $t = t_{acc}$) linearly, and (ii) the pig velocity reaches and remains at its terminal velocity afterwards, $V_{pig} = V_{pigT}$ (for $t > t_{acc}$). The corresponding change in pig location (x_{pig}) is shown in Fig. 5 where it first curves up (for $t < t_{acc}$) to reach $x = L_{acc}$ at $t = t_{acc}$, and then follows a straight-line trend afterwards (for $t > t_{acc}$). Note that such an approximation during the acceleration phase is based on the steady-state interactions among the fluid, pig and pipe wall, and thus makes the model in this study a quasi-steady-state approach (more details on this topic are discussed in the later section).

Once a pig is in motion, the pressure drop across the pig (ΔP_{pig}) can be calculated by using Eqs. (10) through (13). Figs. 6 and 7 show such a result, i.e., ΔP_{pig} as a function of V_{pig} and ΔP_{pig} as a function of q_w, respectively. Because of the nature of quadratic equation in Eq. (10), there exist two solutions - real and imaginary solutions. The real solution, which is physically meaningful, is shown by the colored portion of the curves in Fig. 6 (where the slope is negative) and Fig. 7 (where the slope is positive), while the imaginary solution is shown by the gray portion of the curves

By combining the basic information for the pipeline with a pig (shown in Table 1, and Figs. 4 and 5) and the relationship among ΔP_{pig}, V_{pig} and q_w for the bypass-type pig of interest (shown in Figs. 6 and 7), Fig. 8 shows pressure profile as a function of distance (P vs. x) during the operation time (t). As conjectured from the concept of stiction pressure, there is a threshold value of pressure drop (or inlet pressure, P_{in}) that needs to be overcome for the pig to start its initial motion (ΔP_{pig} = 9.28 MPa (about 1343 psi) approximately at t = 0.2 sec in the figure). As the pig accelerates, ΔP_{pig} decreases (see Fig. 6) and P_{in} reduces continuously until it reaches ΔP_{pig} = 228 kPa (about 33 psi) at $t = t_{acc}$ = 2.0 sec. After the pig reaches its terminal-velocity phase ($t > t_{acc}$), as shown by Fig. 9, P_{in} and ΔP_{pig} do not change any more. Within this phase, it is the pressure values upstream and downstream of the pig (P_{upp} and P_{dnp}) that change with time.

Table 1. Input parameters for the pipeline and pig in the base case.

input parameter	**description**	**value**	**input parameter**	**description**	**value**
R_{pipe} (m)	inner radius of the pipe	0.0486	L_{pig} (m)	length of pig	0.1458
L_{pipe} (m)	total length of the pipe	1300	V_{pigT} (m/s)	pig terminal velocity	1.14
q_{win} (m^3/s)	total flowrate at the inlet	0.00972	δ (m)	gap between pig and pipe wall	0.0001
μ_w (Pa s)	viscosity of driving fluid	0.002	t_{acc} (s)	time for pig to accelerate to V_{pigT}	2
ρ_w (kg/m^3)	density of driving fluid	1000	L_{hole} (m)	length of bypass hole	0.1458
P_{out} (Pa)	backpressure at the outlet	101325	R_{hole} (m)	inner radius of the bypass hole	0.0058
			k	entrance/exit effect	2.95

The results in Figs. 8 and 9 can be used to predict pressure change as a function of time at any longitudinal location (x) along the pipeline. Figs. 10 and 11 show such an example in terms of P_{in}, P_{upp}, and P_{dnp}. As predicted in Fig. 8, Fig. 10 shows that P_{in} first increases up to the threshold pressure value to initiate pig motion, then decreases as the pig accelerates until $t = t_{acc} = 2.0$ sec. P_{in} stays at the same level afterwards ($t > t_{acc}$) maintaining $V_{pig} = V_{pigT}$. Fig. 11 shows details on what happens during the terminal-velocity phase: While P_{in} and P_{out} are fixed at the same level, and P_{upp} and P_{dnp} decrease continuously with time as the pig travels further downstream. Note that ΔP_{pig} (i.e., $P_{upp} - P_{dnp}$) remains the same during this time period.

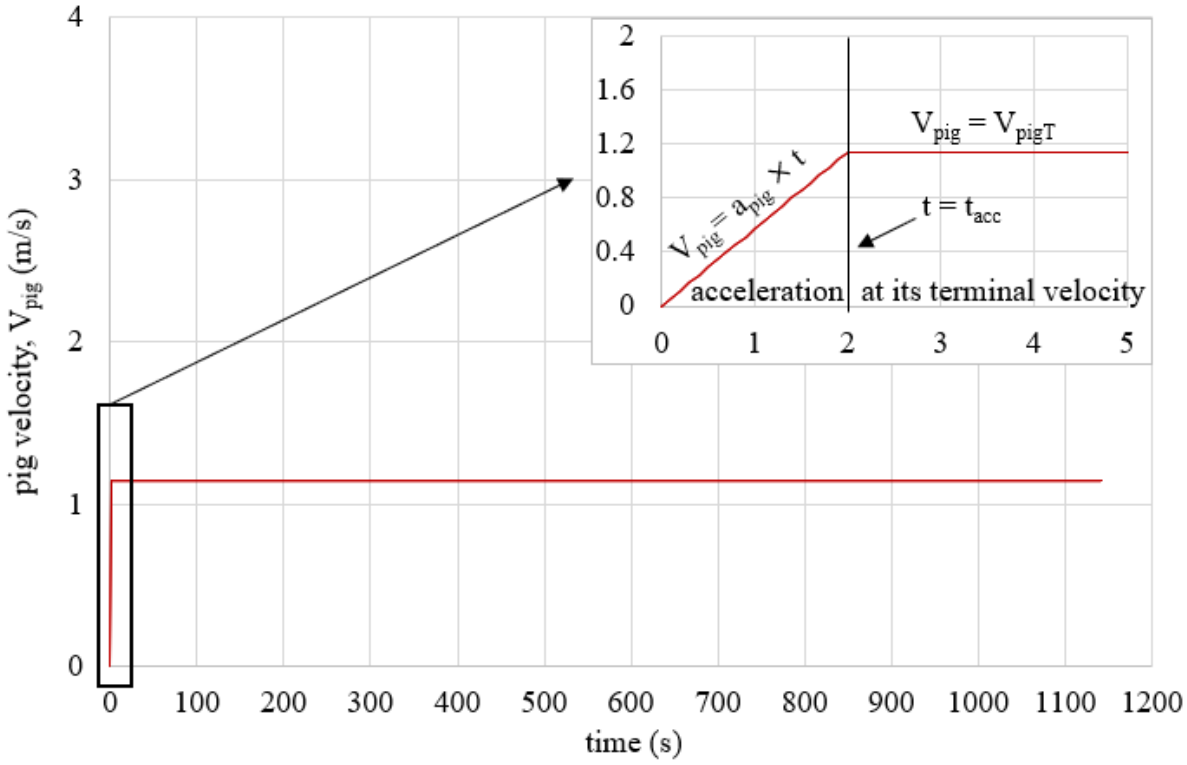

Figure 4. Change in pig velocity (V_{pig}) during acceleration and terminal-velocity phases in the base case.

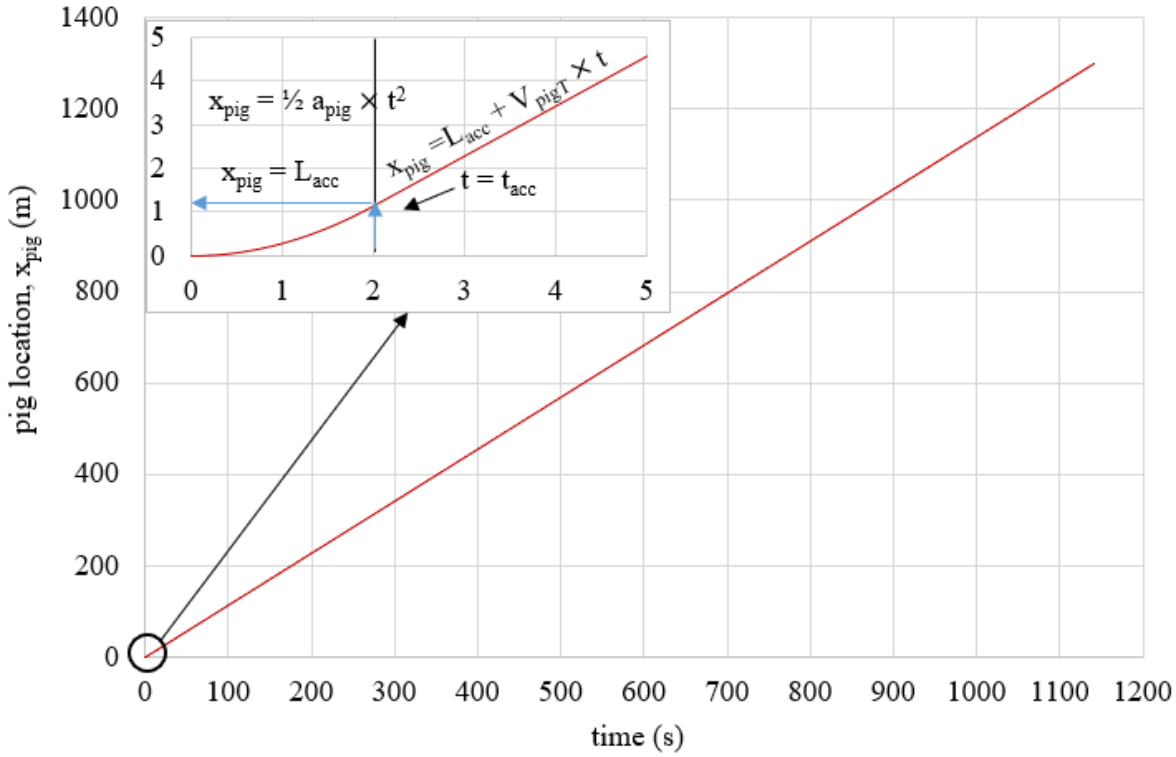

Figure 5. Change in pig location (x_{pig}) during acceleration and terminal-velocity phases in the base case.

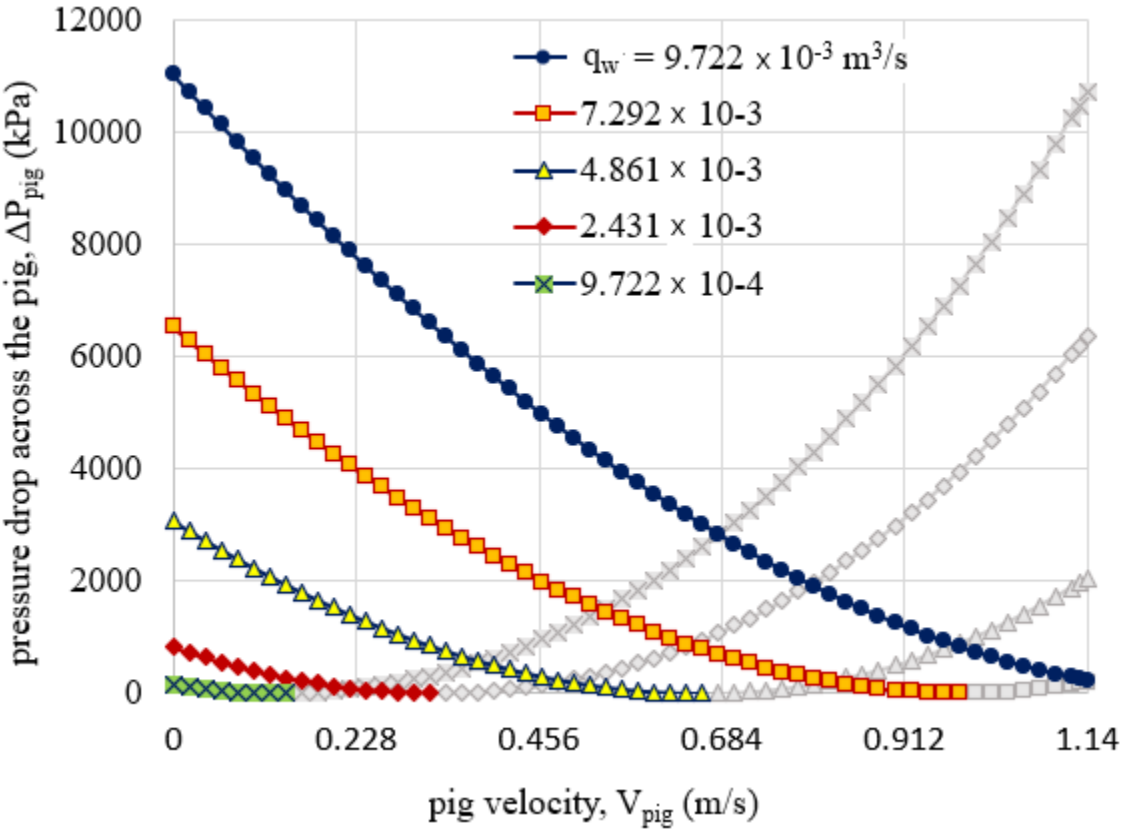

Figure 6. Pressure drop across pig (ΔP_{pig}) as a function of pig velocity (V_{pig}) in the base case (only the colored part of the curves represents real solutions, while the other gray part represents imaginary solutions).

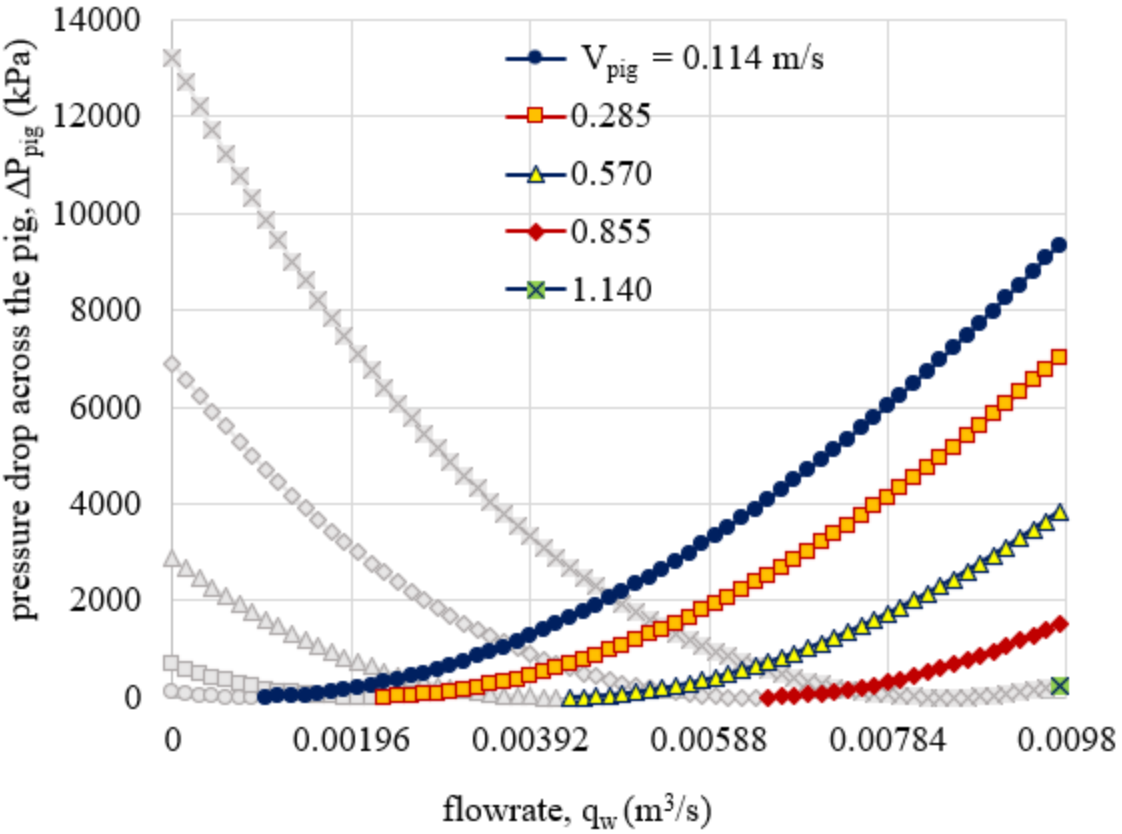

Figure 7. Pressure drop across pig (ΔP_{pig}) as a function of fluid velocity (q_w) in the base case (only the colored part of the curves represents real solutions, while the other gray part represents imaginary solutions).

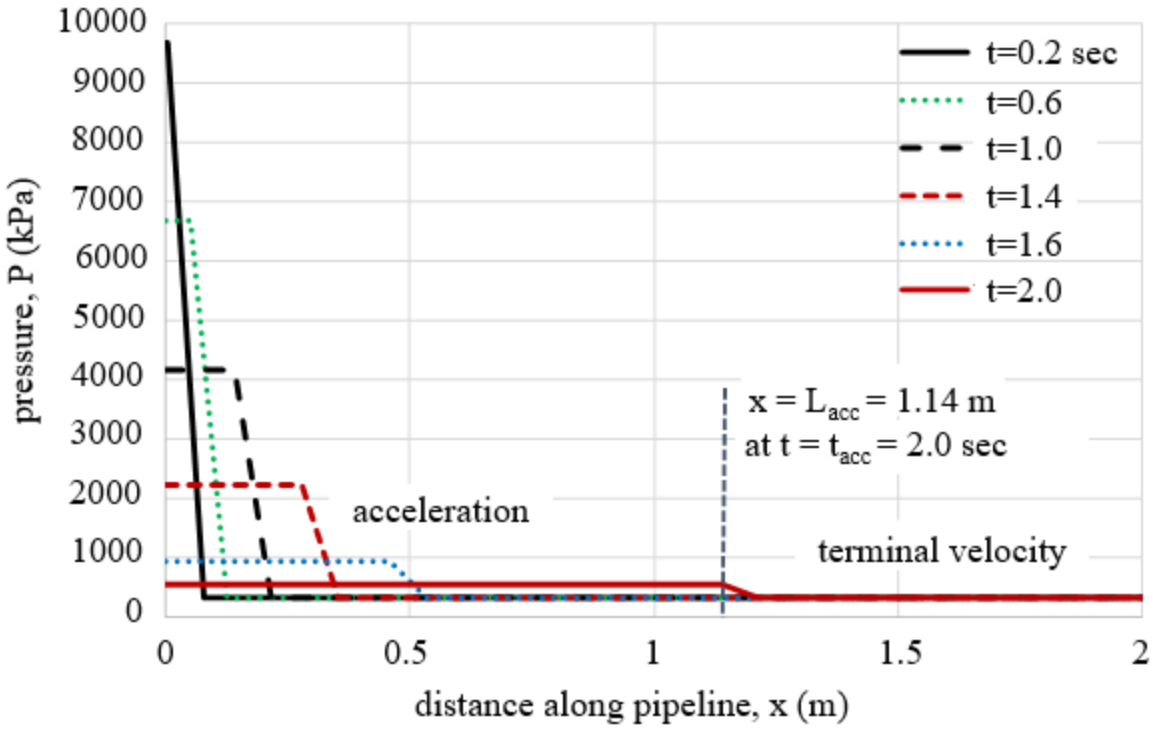

Figure 8. Pressure (P) as a function of longitudinal distance (x) during acceleration and terminal-velocity phases in the base case (P_{out} = 101325 Pa = 14.7 psia).

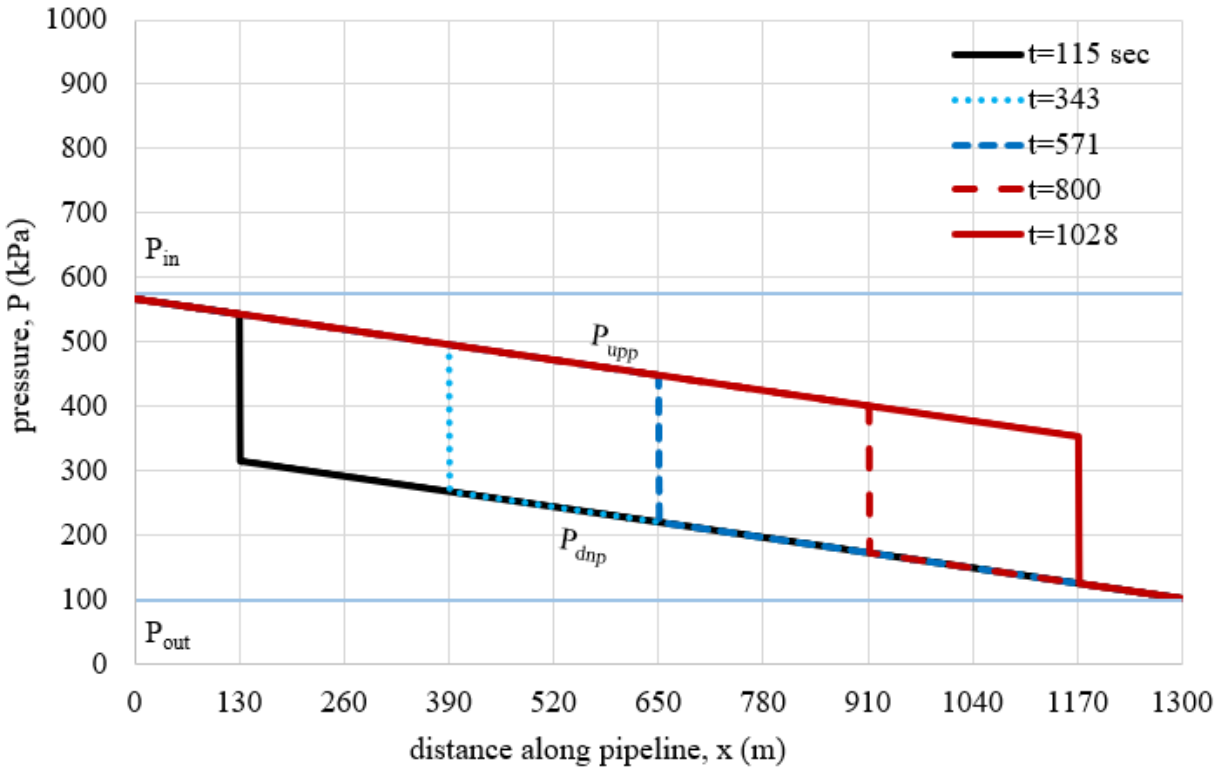

Figure 9. Pressure (P) as a function of longitudinal distance (x) during terminal-velocity phase in the base case (magnified view) (P_{out} = 101325 Pa = 14.7 psia).

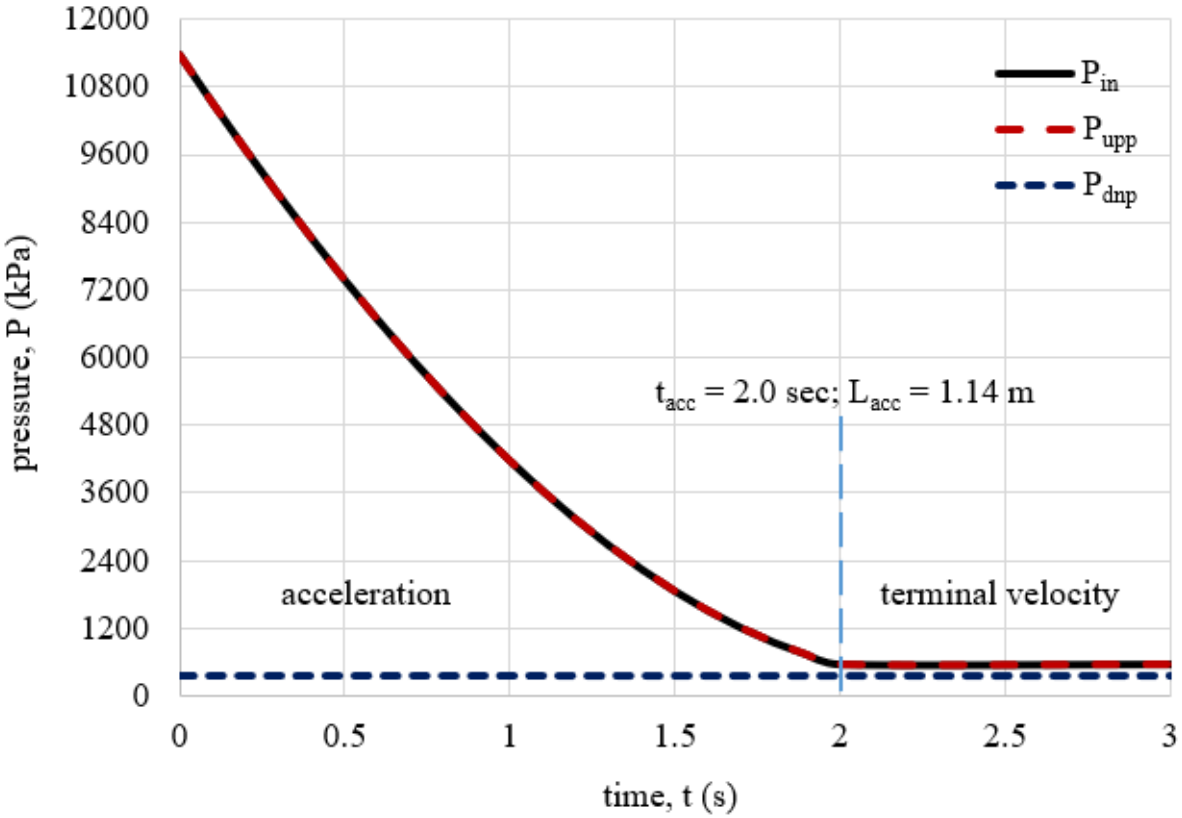

Figure 10. Pressure (P) as a function of time (t) during acceleration and early terminal-velocity phases in the base case (P_{out} = 101325 Pa = 14.7 psia).

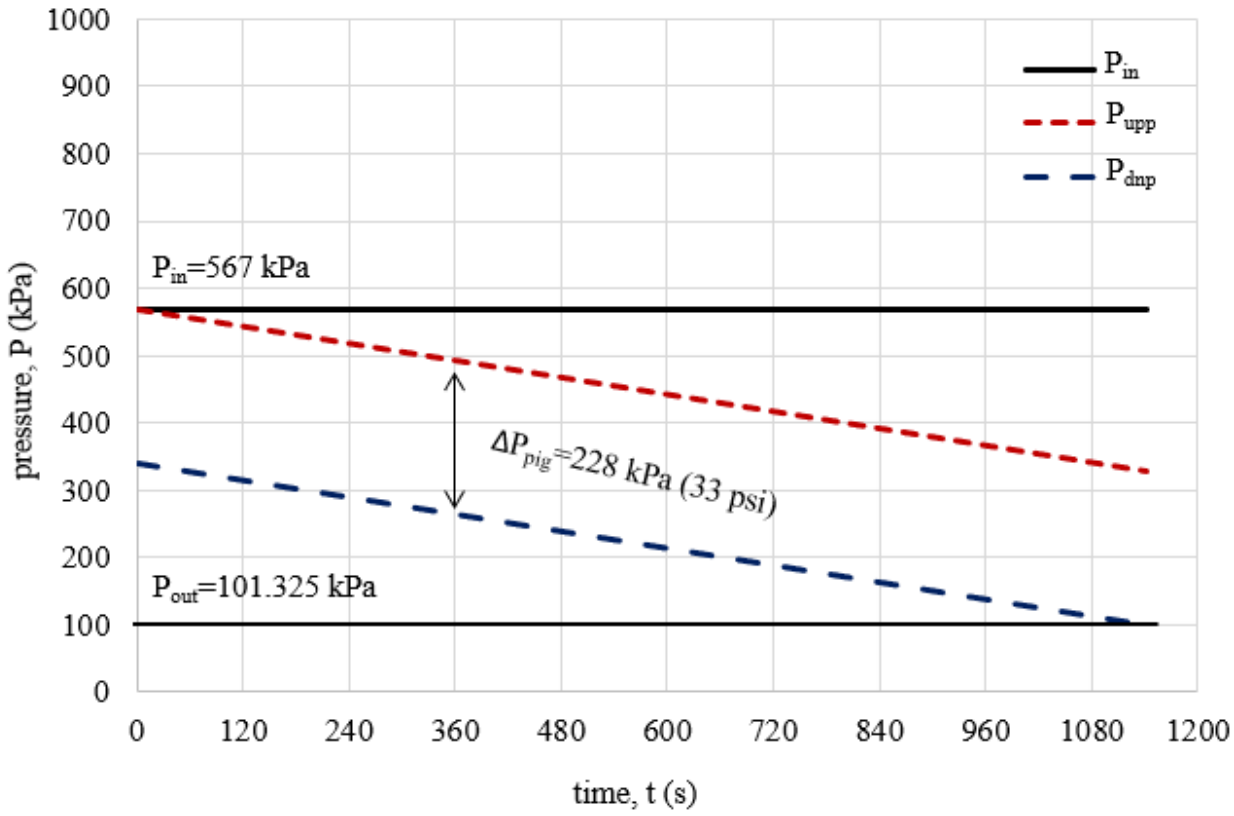

Figure 11. Pressure (P) as a function of time (t) during terminal-velocity phase in the base case (P_{out} = 101325 Pa = 14.7 psia).

The next step of this study is to look into the case with a leak in the system. Table 2 shows input details of the leak: a circular leak opening with the radius (R_{leak}) = 0.6 inch (or 0.007625 m) and the location (x_{leak}) at the midpoint in the total pipeline length (i.e., $L_{pipe}/2$ = 650 m). The model also needs the surrounding pressure outside the leak (P_{surr}) and leak discharge coefficient (c_{leak}). Because t_{acc} = 2.0 sec. is negligible compared to the overall operation time (about 1150 sec. as shown in Fig. 11), this study focuses on the pig motion only during the terminal-velocity phase. The modeling results in the presence of a leak require two separate solutions (when the pig is located upstream of the leak as well as downstream), combining them together.

Figs. 12 through 16 show the calculation results when the pig is located upstream of the leak. First, Fig. 12 presents the relationship between P_{junc} and q_{leak} for the pipeline downstream of

the leak (Eq. (20)) and through the leak (Eq. (22)). The intersection between the two curves (P_{junc} = 181 kPa and q_{leak} = 0.009144 m^3/s for the input parameters shown in Table 1 and Table 2) are obtained by iterations. The results are summarized by the schematic figure in Fig. 13.

Those subsequent plots show the pressure as a function of distance x (Fig. 14, showing the results at three different times and the pig arrival time of t = 566 sec at the leak), the pressure-gradient (dP/dx) as a function of x at t = 343 sec (Fig. 15), and the change in pressure as a function of time at different locations (P_{in}, P_{upp}, and P_{dnp}). Overall, these are similar to Figs. 9 and 11 because the pig is still in the upstream of the leak during which q_{win} and V_{pig} are the same as no-leak base-case scenario. Some interesting aspects should be noted, however, such as (i) the pressure gradient along the upstream pipeline (183 Pa/m) is higher than that along the downstream pipeline (122 Pa/m) because of fluid loss through the leak and (ii) the pressure loss across the pig plays a significant role compared to the overall pressure drop along the fluid in the pipeline (see ΔP_{pig} in Fig. 14). Such an aspect is also shown by the pressure gradient (see $\Delta P_{pig}/L_{pig}$) in Fig. 15.

Table 2. Input parameters for the pig.

input parameter	**description**	**value**
R_{leak} (m)	radius of the leak	0.00763
x_{leak} (m)	longitudinal leak location	650
P_{surr} (Pa)	external pressure surrounding the leak	101325
c_{leak}	discharge coefficient	0.85
t_{acc} (s)	time for pig to accelerate to V_{pigT}	0*
*t_{acc}=0 means the pig moves at its terminal velocity.		

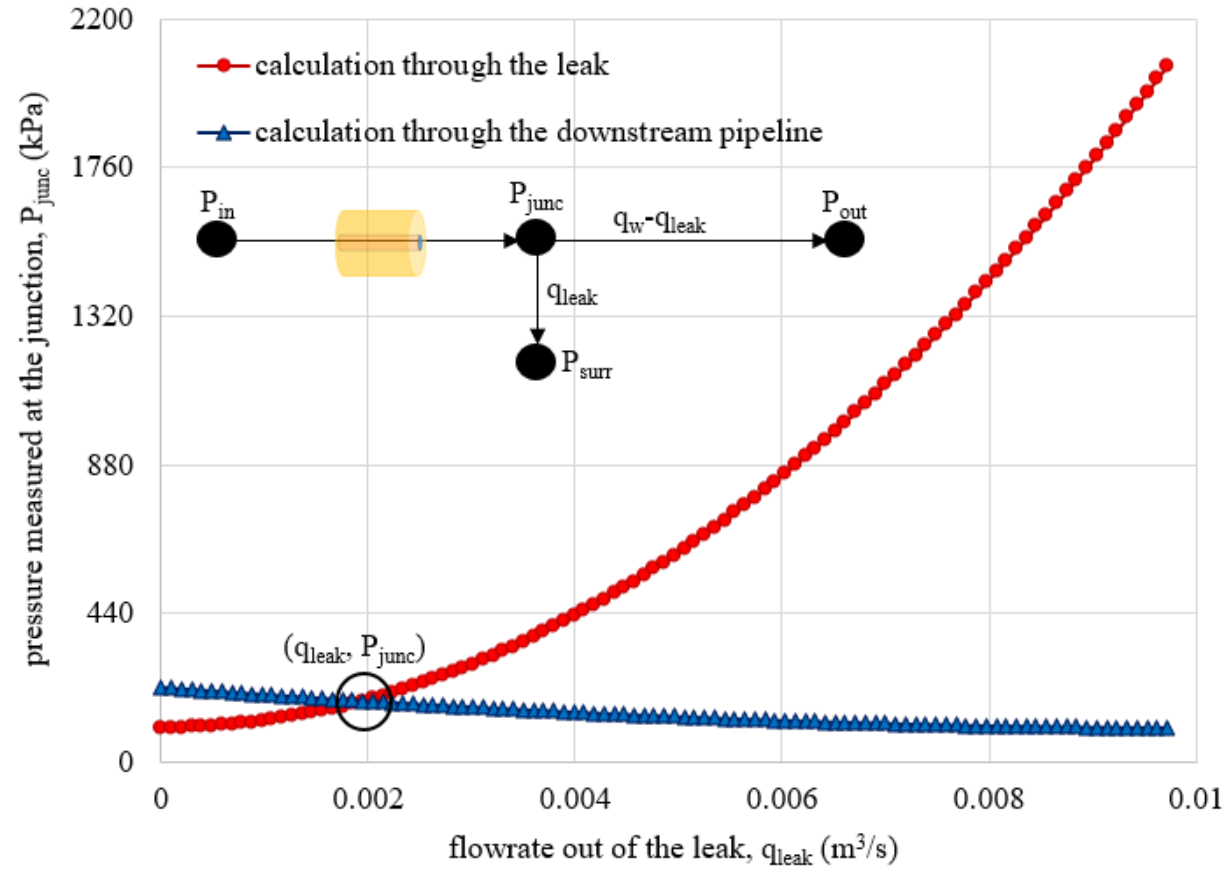

Figure 12. Finding junction pressure (P_{junc}) and leak flowrate (q_{leak}) when the pig is upstream of the leak location (Pig terminal velocity upstream of the leak (V_{pigT} = 1.14 m/s); iterations are used to find the intersection point of (q_{leak}, P_{junc})).

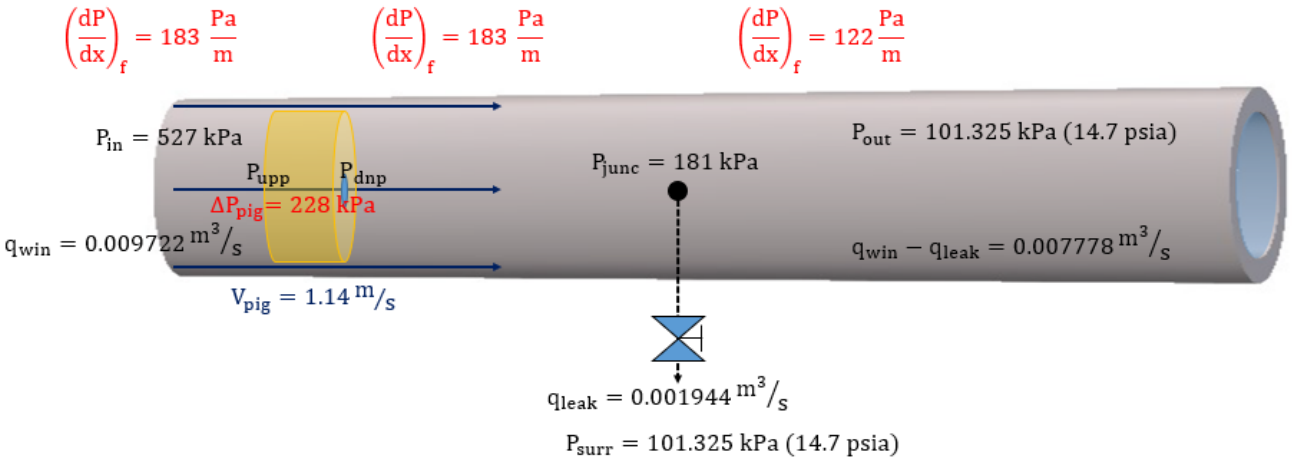

Figure 13. A schematic figure summarizing calculation results when the pig is upstream of the leak location.

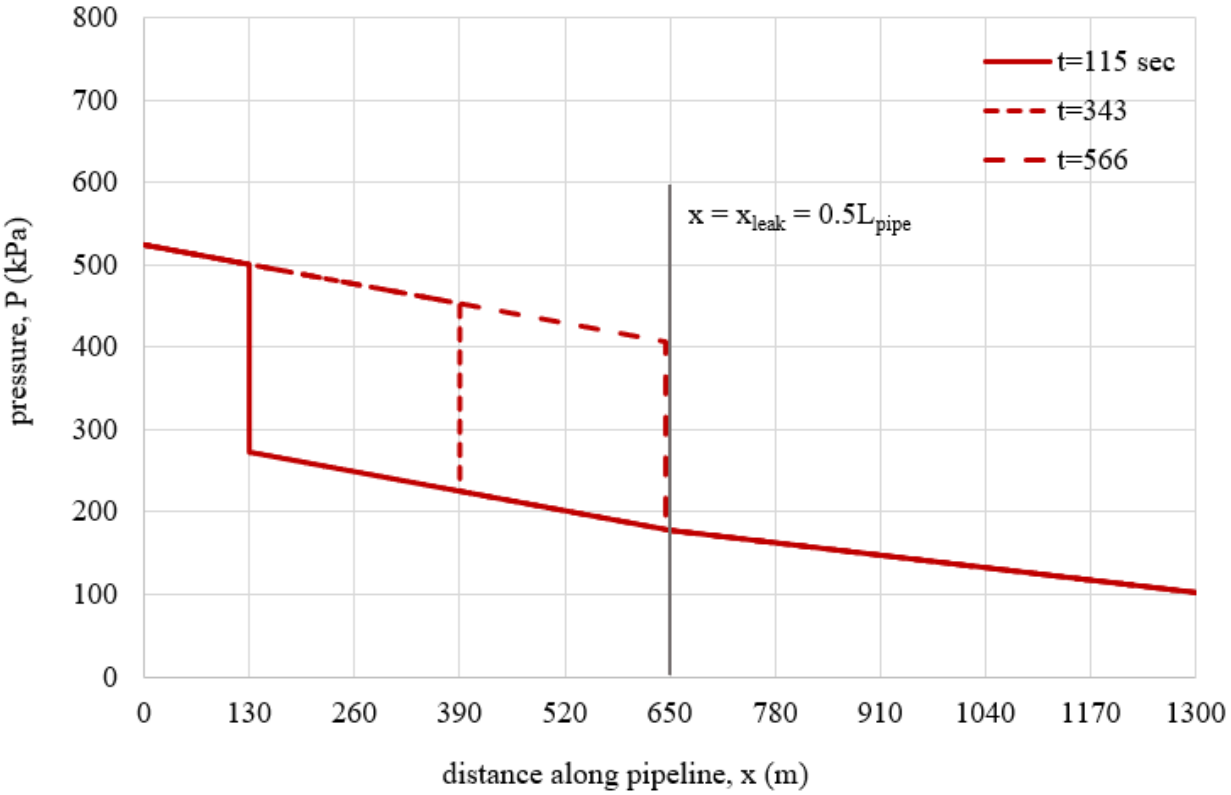

Figure 14. Pressure (P) as a function of longitudinal distance (x) when the pig is upstream of the leak location.

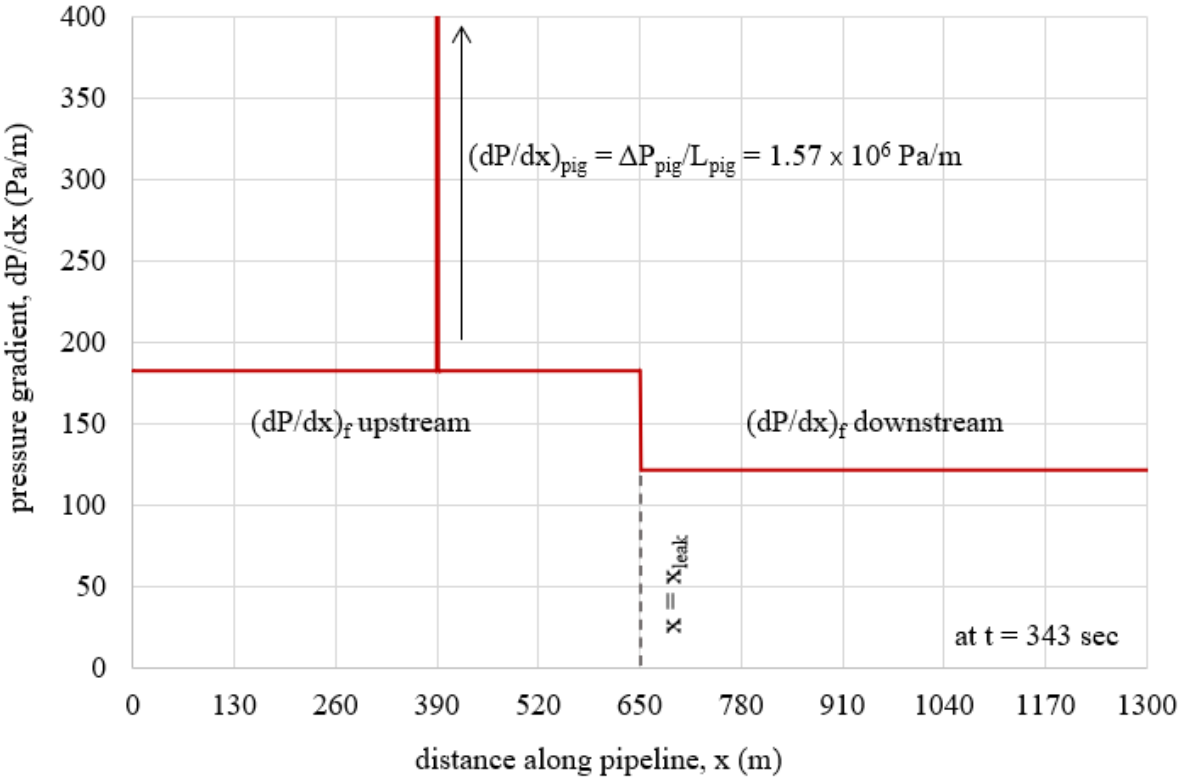

Figure 15. Pressure gradient (dP/dx) as a function of longitudinal distance (x) when the pig is upstream of the leak location.

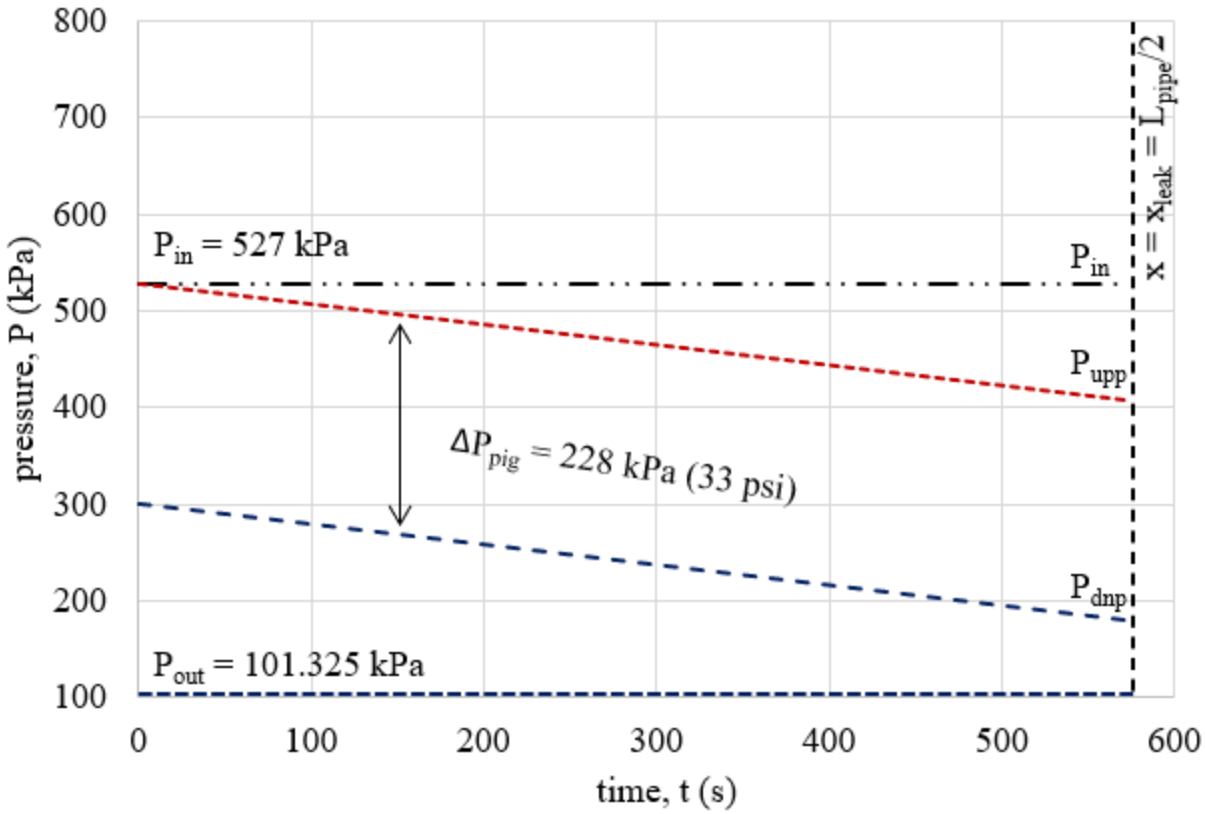

Figure 16. Pressure (P) as a function of time (t) when the pig is upstream of the leak location.

Figs. 17 through 21 show the calculation results when the pig is located downstream of the leak. It should be noted that, similar to the case with the pig upstream, the calculation requires the downstream terminal velocity that can initially be estimated or measured from the experiments. This section chooses the downstream terminal velocity (V_{pigTdn}) ¾ of the upstream terminal velocity (V_{pigT}), which means V_{pigTdn}/V_{pigT} = 0.75, or V_{pigTdn} = 0.855 m/s (2.81 ft/s). Different ratios of V_{pigTdn}/V_{pigT}, of course, affect pressure losses and thus leak flowrate, which is discussed more in the later section.

First, Fig. 17 presents the relationship between P_{junc} and q_{leak} along the pipeline (Eq. (25)) and through the leak (Eq. (22)). The intersection between the two curves, when the pig is located downstream, gives P_{junc} = 230 kPa and q_{leak} = 0.00272 m^3/s (cf. P_{junc} = 181 kPa and q_{leak} = 0.009144 m^3/s in Fig. 12). The results are summarized by the schematic figure in Fig. 18 that can be contrasted with Fig. 13.

Similarly, Fig. 18 shows the results of pressure as a function of distance (at three different times) right after the pig passes the leak location (t =578 sec), Fig. 19 the pressure-gradient (dP/dx) as a function of x at t = 876 sec, and Fig. 20 the change in pressure as a function of time at different locations (P_{in}, P_{upp}, and P_{dnp}). Overall, they are similar to Figs. 14 and 16 (when the pig located upstream of leak) with some notable differences such as (i) the pressure loss across the pig is reduced (ΔP_{pig} = 63 kPa (9 psi) from 228 kPa (33 psi)) because of the change in flowrate across the pig (q_{win} - q_{leak} = 0.007002 m^3/s from q_{win} = 0.009722 m^3/s) and (ii) the inlet pressure (P_{in}) changes to and maintained at 348 kPa (from 527 kPa), accordingly, as the pig passes through the leak location.

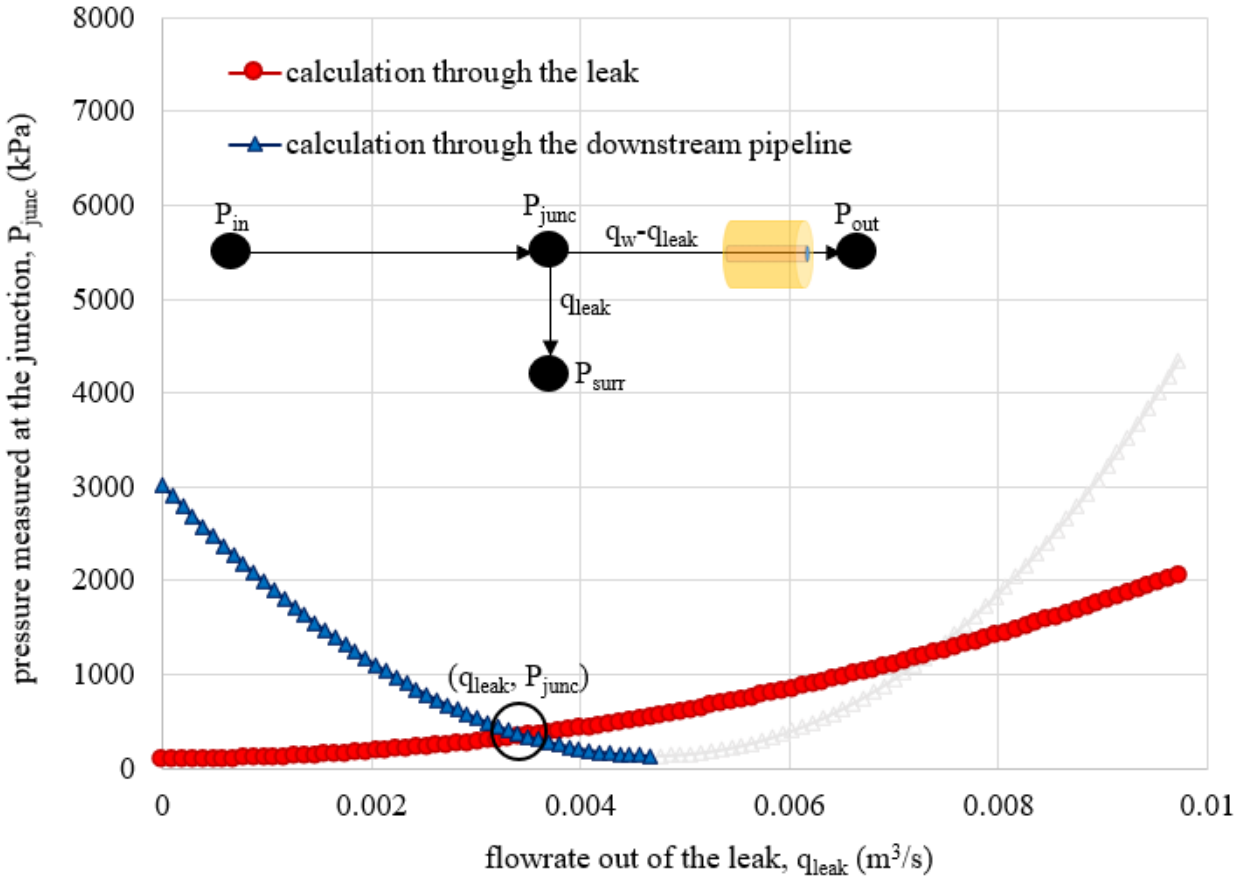

Figure 17. Finding junction pressure (P_{junc}) and leak flowrate (q_{leak}) when the pig is downstream of the leak location (Pig terminal velocity downstream of the leak is 75% of that upstream (V_{pigTdn}/V_{pigT} = 0.75); iterations are used to find the intersection point of (q_{leak}, P_{junc})).

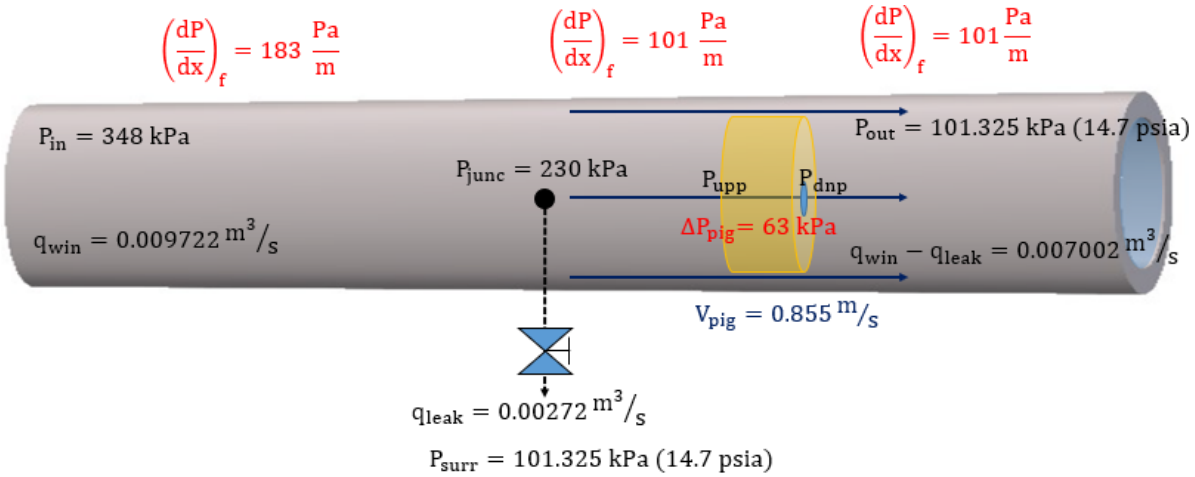

Figure 18. A schematic figure summarizing calculation results when the pig is downstream of the leak location.

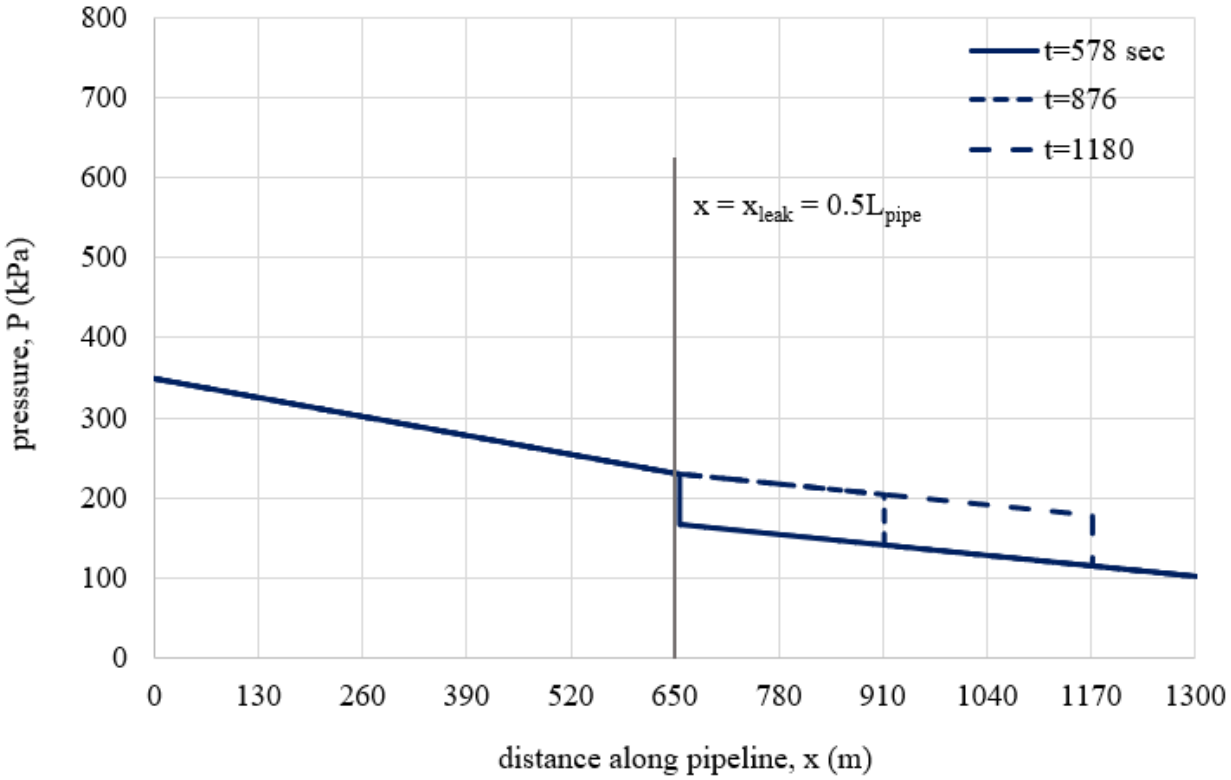

Figure 19. Pressure (P) as a function of longitudinal distance (x) when the pig is downstream of the leak location.

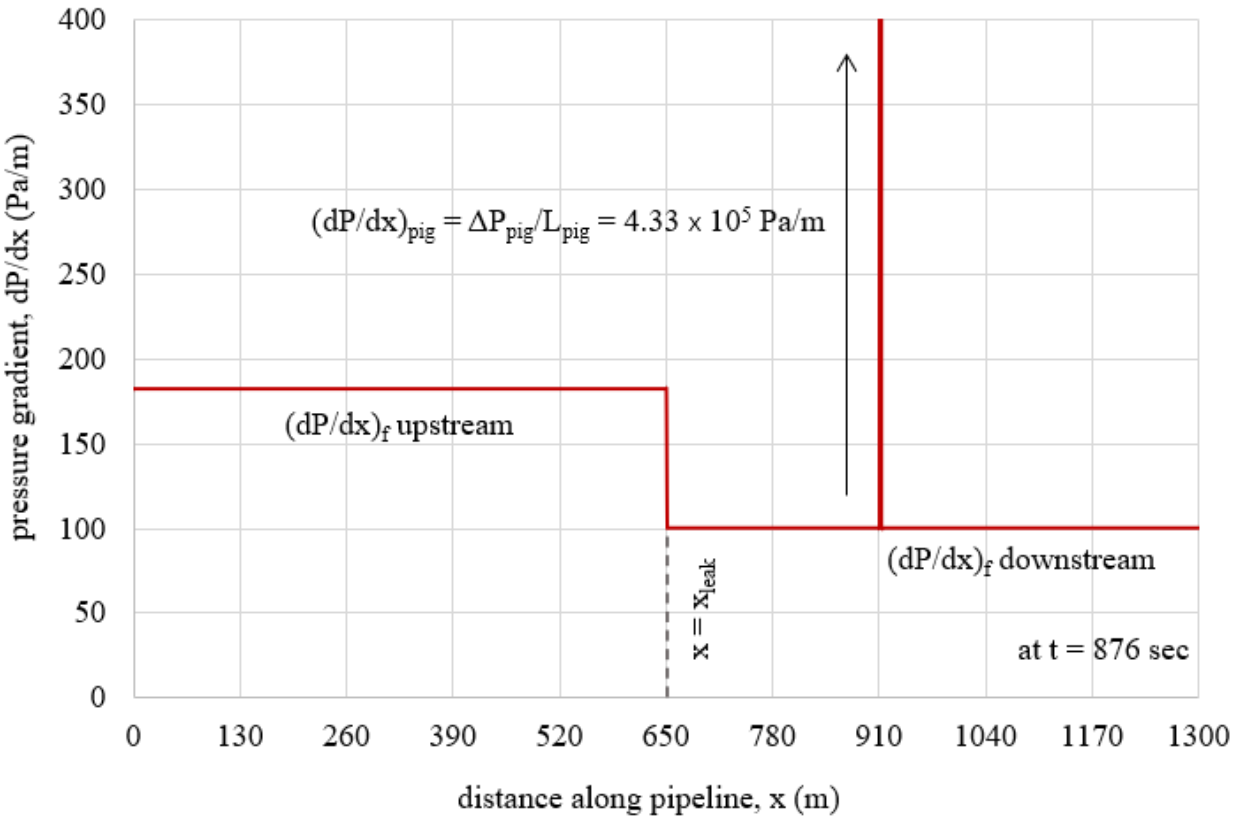

Figure 20. Pressure gradient (dP/dx) as a function of longitudinal distance (x) when the pig is downstream of the leak location.

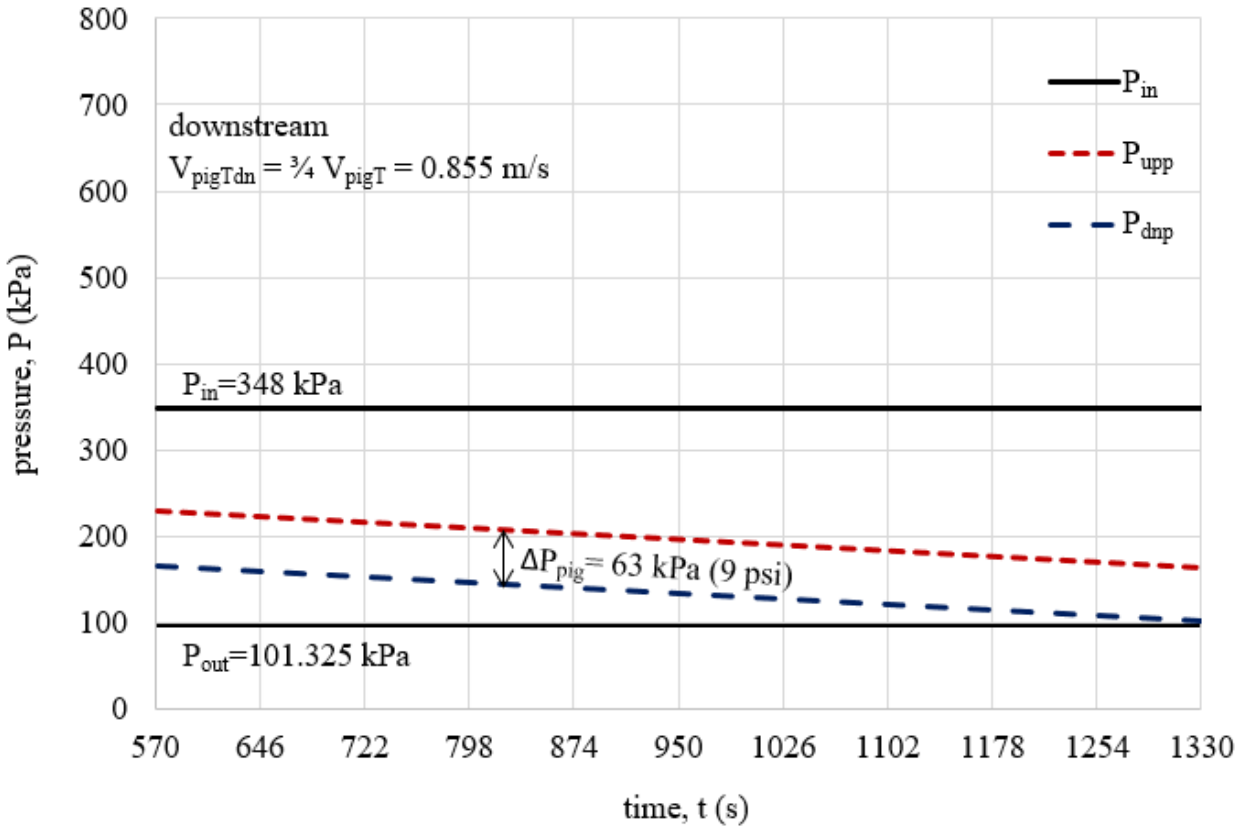

Figure 21. Pressure (P) as a function of time (t) when the pig is downstream of the leak location.

Putting both results (the pig upstream and downstream) together, a complete description of the pig travelling over the pipe length can be created. First, Fig. 22 shows six different pig locations (related to six different times, equivalently) where the results are reported, first three when the pig is located upstream (x_{pig} = 0.1L_{pipe}, 0.3L_{pipe}, and 0.5L_{pipe} -L_{pig}) and the other three when the pig is located downstream (x_{pig} = 0.5L_{pipe}, 0.7L_{pipe}, and 0.9L_{pipe}). Figs. 23 and 24 show the combined solutions, when the pig travels upstream as well as downstream (i.e., Figs. 16 and 19 and Figs. 18 and 21), respectively.

Finally, Figs. 25 through 27 show how pressure changes as a function of distance and time when the pig terminal velocity downstream is 60 %, 70 %, and 90 % of that upstream (i.e., V_{pigTdn}/V_{pigT} = 0.6, 0.7, and 0.9, respectively; note that V_{pigTdn}/V_{pigT} = 0.75 in Figs. 23 and 24). Because ΔP_{pig}, V_{pig} and q_w are interconnected (see Figs. 6 and 7), a change in pig velocity (whether upstream or downstream of the leak) leaves unique pressure signatures as shown in Figs. 25 through 27. Note that the higher V_{pigTdn}/V_{pigT}, the lower ΔP_{pig} downstream, and, as a result, the more reduction in P_{in} as the pig moves from upstream to downstream.

These results show the significance of this study as active smart-pig leak-detection method where the pressures measured in both ends of the pig while traveling (i.e., P_{upp} and P_{dnp}) can greatly improve traditional passive leak-detection methods based only on the pressure and/or flowrate measurements at the inlet and outlet (i.e., P_{in} and P_{out}; q_{win} and q_{wout}). As shown by the pressure signatures in Figs. 23 through 27, for example, the sharp changes in P_{in} and ΔP_{pig} (or, P_{upp} - P_{dnp}), as the pig travels across the leak location, can be used as an indicator of x_{leak}. Furthermore, the magnitude of the change in ΔP_{pig}, measured in the experiments, can also be used to confirm the change in pig velocity (i.e., V_{pigT} to V_{pigTdn}) and thus pig arrival time at the outlet. These pig velocities, of course, can be measured directly (as a part of smart pig capacity) or estimated from the experimental data.

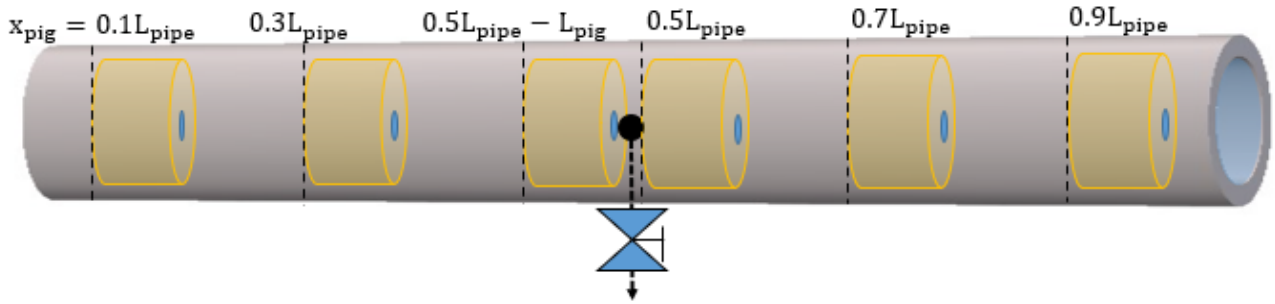

Figure 22. Six different pig locations selected to create pressure profile (x_{pig} = $0.1L_{pipe}$, $0.3L_{pipe}$, $0.5L_{pipe}$ -L_{pig}, $0.5L_{pipe}$, $0.7L_{pipe}$, and $0.9L_{pipe}$).

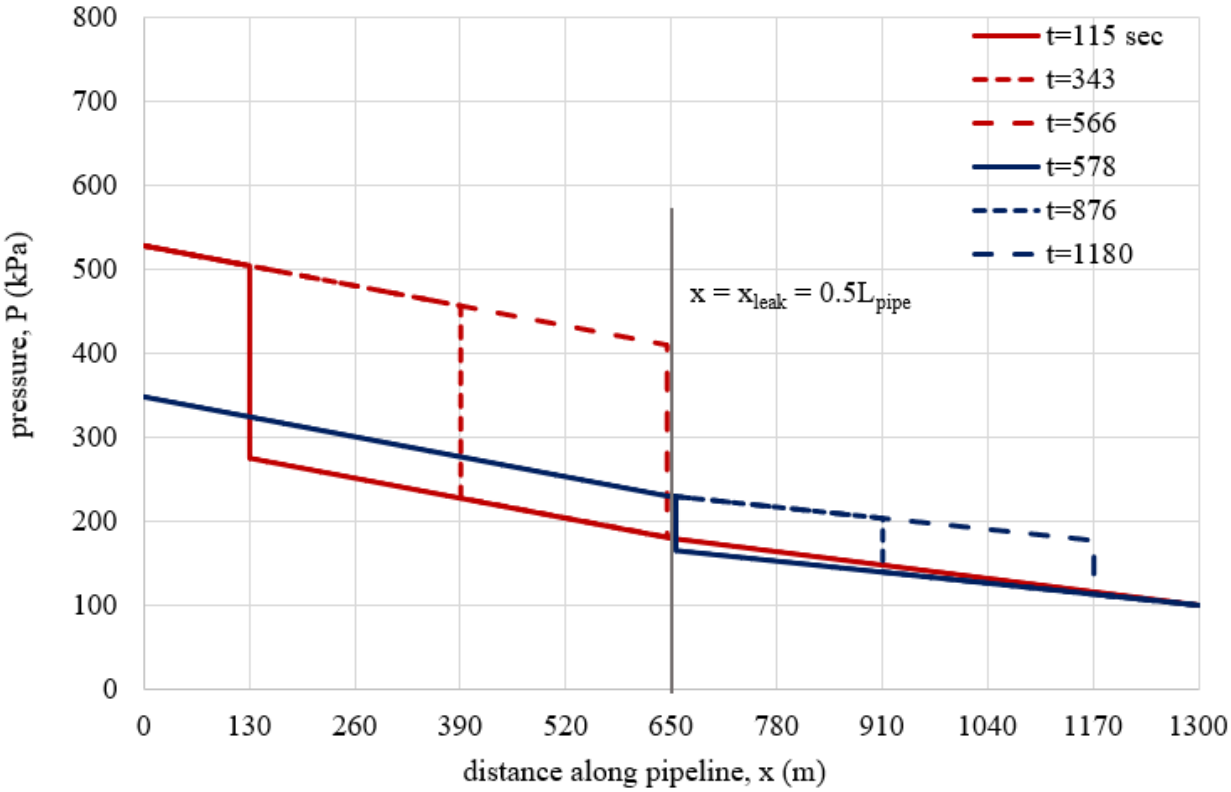

Figure 23. Pressure (P) as a function of longitudinal distance (x) as pig travels the entire pipe length (Pig terminal velocity downstream is 75% of that upstream (VpigTdn/VpigT = 0.75)).

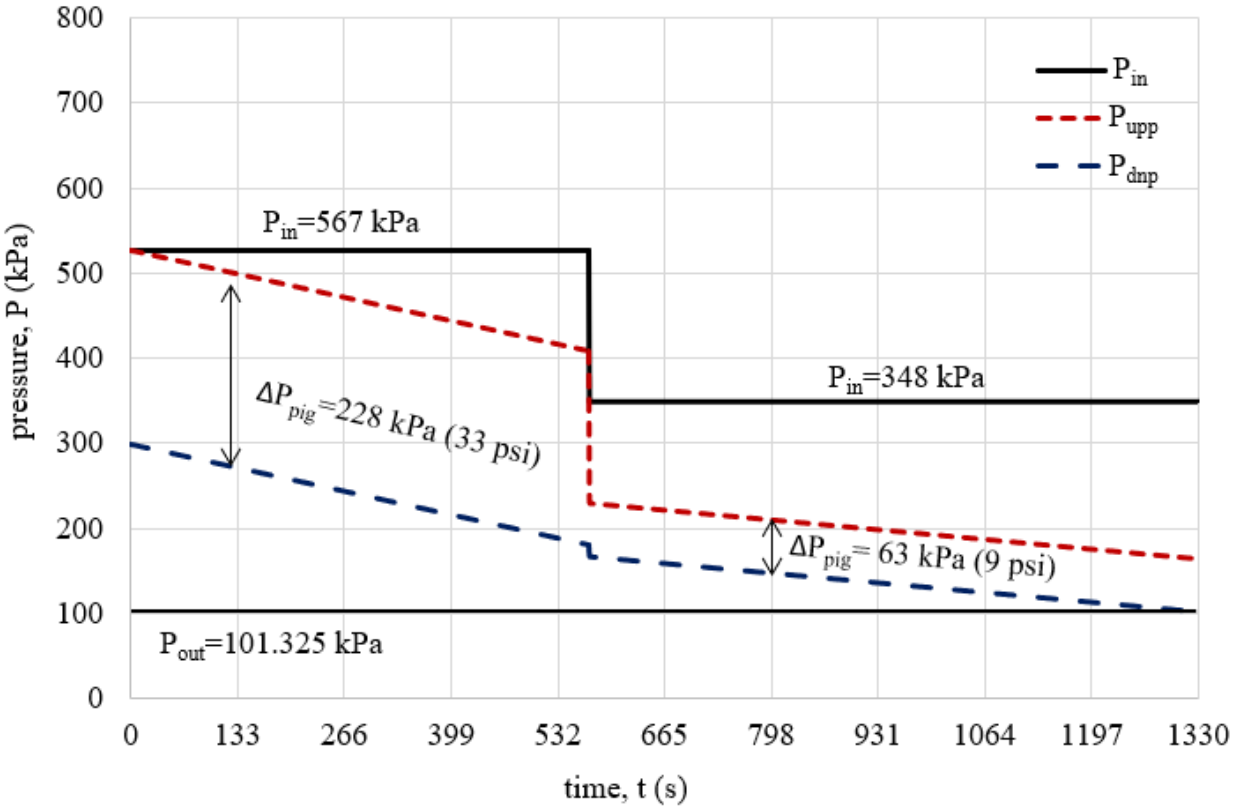

Figure 24. Pressure (P) as a function of time (t) as pig travels the entire pipe length (Pig terminal velocity downstream is 75% of that upstream (V_{pigTdn}/V_{pigT} = 0.75)).

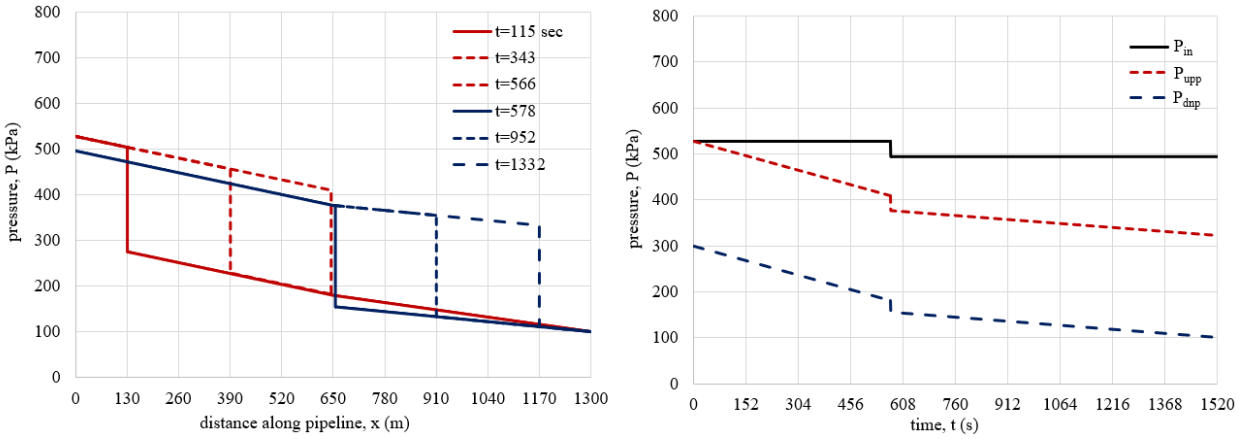

Figure 25. Pressure (P) as a function of longitudinal distance (x) and time (t) as pig travels the entire pipe length (Pig terminal velocity downstream is 60% of that upstream (V_{pigTdn}/V_{pigT} = 0.6)).

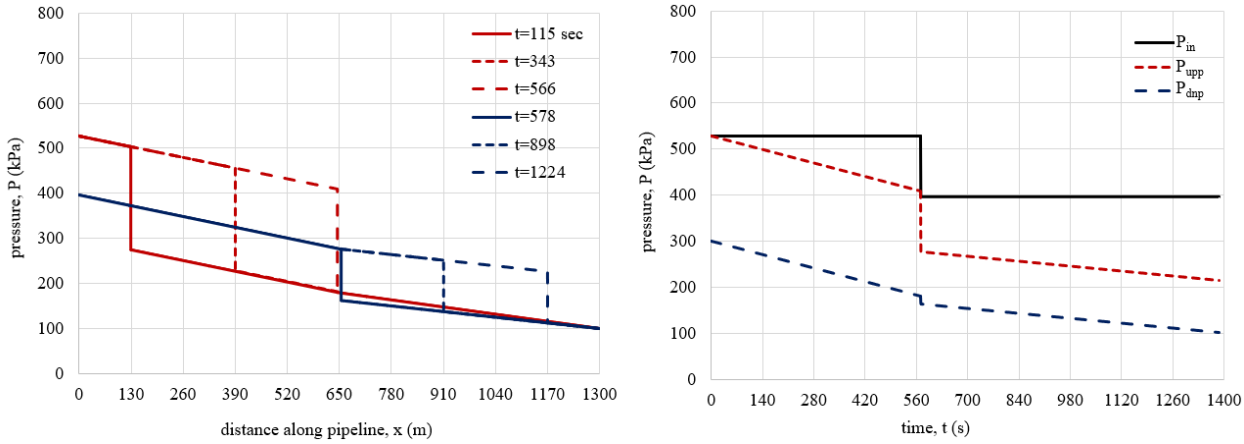

Figure 26. Pressure (P) as a function of longitudinal distance (x) and time (t) as pig travels the entire pipe length (Pig terminal velocity downstream is 70% of that upstream (V_{pigTdn}/V_{pigT} = 0.7))

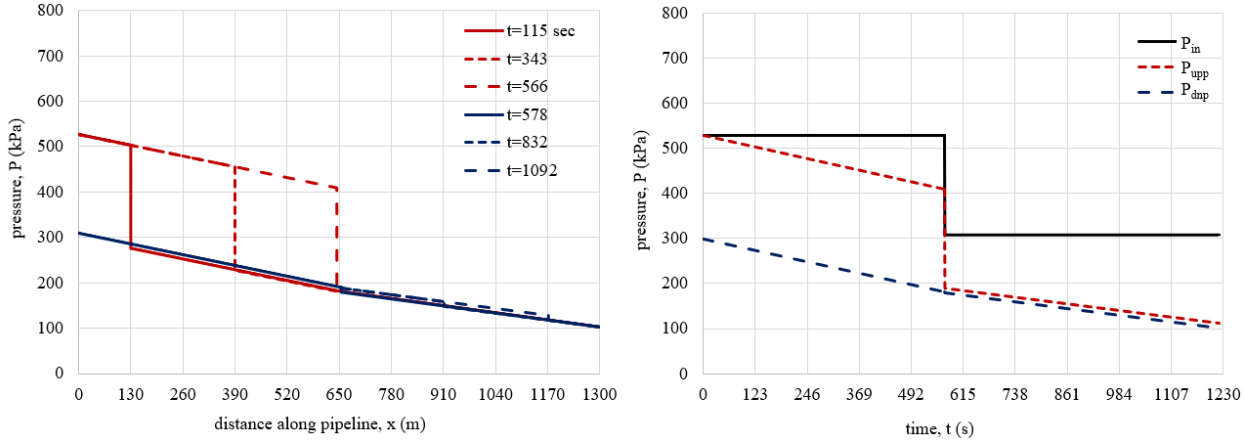

Figure 27. Pressure (P) as a function of longitudinal distance (x) and time (t) as pig travels the entire pipe length (Pig terminal velocity downstream is 90% of that upstream (V_{pigTdn}/V_{pigT} = 0.9)).

Such results in terms of pressure signature (Figs. 23 through 27), if estimated or obtained experimentally, can be applied to determine leak flowrate (q_{leak}) and junction pressure (P_{junc}) at the leak location (x_{leak}). For example, the case shown in Figs. 23 and 24 (where $V_{pigTdn}/V_{pigT} = 0.75$ with $V_{pigT} = 1.14$ m^3/sec (Table 1)), has q_{leak} and P_{junc} values of 0.00194 m^3/sec and 181 kPa when the pig is upstream of the leak (Fig. 12) and 0.00272 m^3/sec and 230 kPa when the pig is downstream of the leak (Fig. 17).

When the pig terminal velocity downstream is 60%, 70%, and 90% of that upstream (i.e., $V_{pigTdn}/V_{pigT} = 0.6$, 0.7, and 0.9, respectively; Figs. 25 through 27), the q_{leak} and P_{junc} values are 0.00340 m^3/sec and 375 kPa; 0.00301 m^3/sec and 275 kPa; and 0.00204 m^3/sec and 190 kPa when the pig is downstream of the leak. The q_{leak} and P_{junc} values, when the pig is upstream, are not affected and therefore stay same, however. Note that the lower V_{pigTdn}/V_{pigT}, the higher q_{leak}.

In actual lab experiments and field tests with a smart pig, q_{leak} and ΔP_{leak} (i.e., $P_{junc} - P_{surr}$) can readily be estimated from pressure signatures. Therefore, size (d_{leak}) is then determined by q_{leak} and ΔP_{leak} (Eq. (26)).

DISCUSSIONS

The modeling approach implemented in this study is based on quasi-steady state, *per se*, because the calculation during the pig set in motion is based on the steady-state relationships among the pressure drop across the pig (ΔP_{pig}), water flow rate (q_w), and pig velocity (V_{pig}). In order to check the validity of the model, one can perform a transient simulation for the pig movement. Fig. 28 shows example simulation results from OLGA where the same input parameters (such as pipeline dimensions, fluid properties, and injection and outlet conditions) are applied. Because OLGA provides only cylindrical pig (i.e., pig with gaps but no holes), this simulation effort adjusts a pig friction factor that offers a similar pressure drop across the pig. Please note that, as a result, the simulation outputs are produced not to confirm the accuracy of the quasi-steady-state modeling, but to confirm the general trend.

First, the simulation performs a single-phase water flow in a horizontal pipeline from t = 0 sec during which the pressure gradient along the pipeline remains low and constant and the inlet pressure is maintained almost at a fixed value. The pig is launched at t = 900 sec, accelerates until t = 1360 sec to reach a terminal velocity, and then exits the system at t = 2290 sec. Overall, the transient simulation results resemble the quasi-steady-state modeling results. For example, during the acceleration phase (about $900 < t < 1360$ sec), pig velocity (V_{pig}) increases with time which leads to a steep reduction in ΔP_{pig} and P_{in}. During the terminal-velocity phase (about $1360 < t < 2290$ sec), ΔP_{pig} and P_{in} stay at the same level, and the high pressure-gradient wave across the pig propagates linearly with time. The only difference between the quasi-steady-state modeling and the transient simulation seems to be the way the pig accelerates during the acceleration phase, i.e., more gradually taking longer time to reach the terminal velocity in the transient simulation. This

makes sense because the simulation has the capacity of taking the dynamics between the fluid, pipe wall, and pig surface into account in a time-dependent manner.

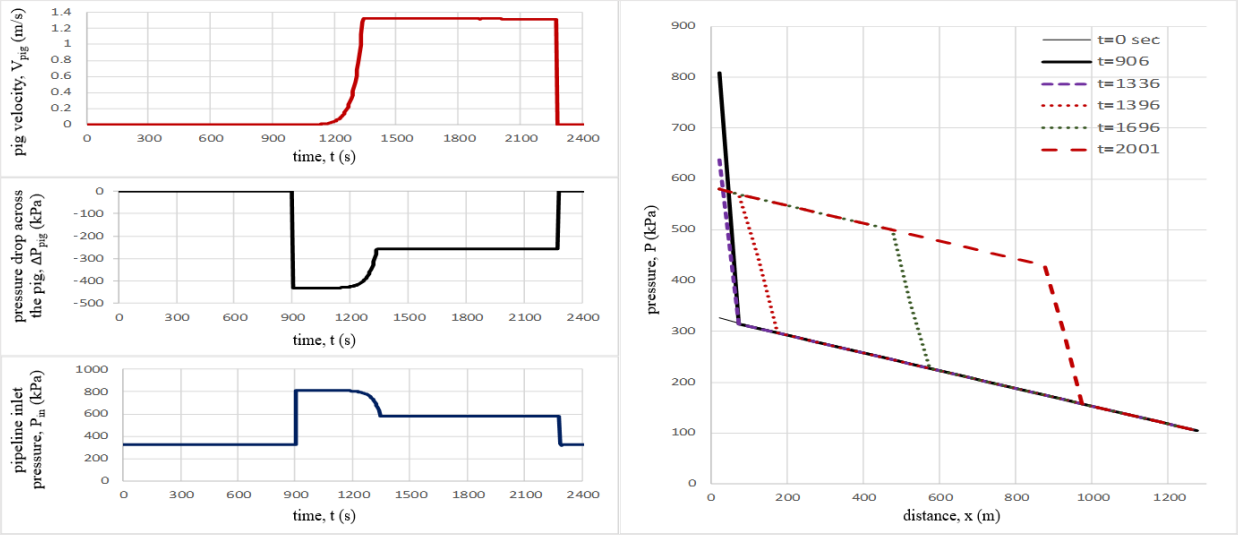

Figure 28. Transient OLGA simulation to validate the model in this study (similar input parameters with incompressible single-phase water).

Another aspect that can be examined by the transient simulation is pig motion when multiphase-phase flow and compressible fluid are associated. Such cases are obviously beyond the scope of this study (i.e., incompressible single-phase flow) for leak-detection purpose, but one may get a useful insight as a part of future work.

Fig. 29 repeats the same simulation case as Fig. 28 including injection rate at the inlet, except that the fluids now consist of 20 % of air and 80 % of water in terms of mass. The results show two main differences compared with the incompressible single-phase flow (Fig. 28). First, the presence of compressible gas phase makes the pressure profile (i.e., pressure vs. distance) curved showing the effect of gas-phase decompression towards the outlet, and accordingly the inlet pressure is much higher to compress the gas phase to get the same injection rate. Second, the transient simulation exhibits a higher level of fluctuation in terms of pig velocity and pressure drop that may sometimes cause convergence and stability issues. Because the trend observed with

multiphase flow, including a compressible phase is similar to what is predicted with the modeling results in this study, the extension of similar leak-detection methods in a compressible multiphase flowline appears to be promising.

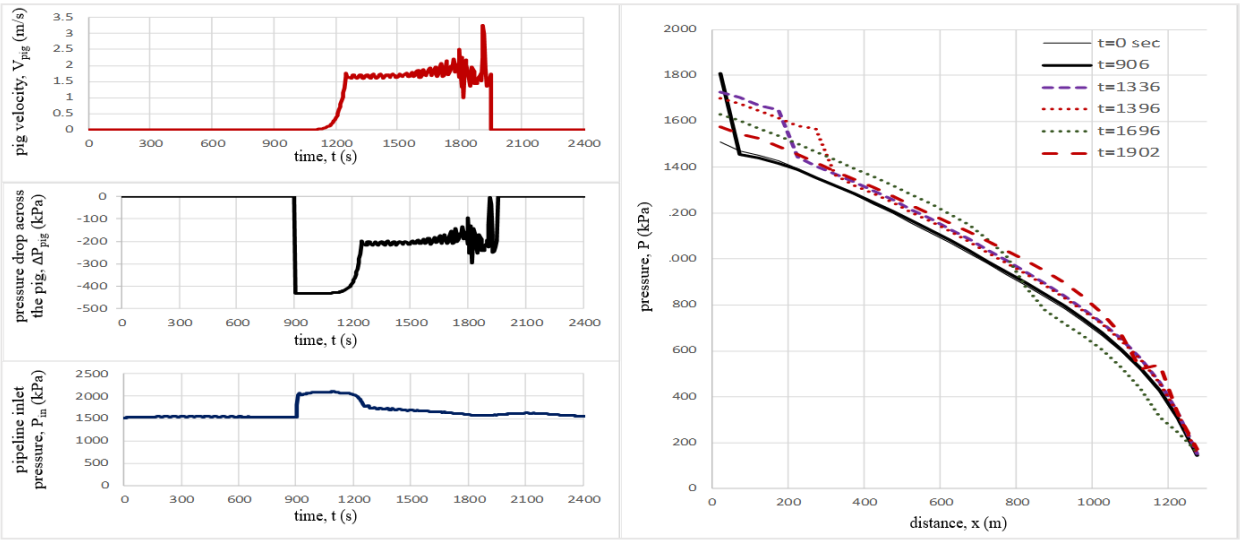

Figure 29. Transient OLGA simulation to understand multiphase-flow and compressibility aspects (similar input parameters, keeping the same total flowrate at the inlet with 20% air and 80% water).

The results obtained in this study based on the quasi-steady-state approach and the results from transient simulations (compressible vs. incompressible phases; single-phase vs. multiphase flow) can be used to guide experimental studies to come as a next phase. The experimental design can be made with a long pipeline that is coiled in circles. For each circle of the pipeline, a pressure transducer and a leak can be installed to measure pressure responses and mimic various leak conditions. It should be noted that this modeling study may be yet to be ready for the field testing, where the pipe inner surface may not be clean (because of corrosion and erosion, for example), where the pipe inner diameter may not be uniform (because of pipe deformation and solid deposition), and where the fluid flow and pig motions are complicated (multiphase flow,

incompressible flow, complex terrain with varying inclination angles, pig not reaching the terminal-velocity phase and so on).

Limited cursory trials with transient simulator can be performed with the addition of pipeline inclination angle. Some preliminary results show that pipeline inclination angle leads to the change in overall pressure drop along the pipeline due to the addition of hydrostatic pressure. There appears almost no change in pressure drop across the pig (ΔP_{pig}) or pig velocity (V_{pig}), however, because the length scale of the pig is negligible compared to that of pipeline. In general, the effect of upward pipeline inclination on leak detection seems to help leak detection because the pressure drop across the leak is higher in that case. Additional work is required to investigate more complicated pipeline configurations associated with various inclinations angles.

Finally, the effects of those modeling parameters for the quasi-steady-state approach in this study need to be investigated for a wide range of scenarios. They include, but are not limited to, different pig characteristics (gap size, bypass hole diameter, etc.), pig types, and pig materials. It is because the pig dynamics may be highly influenced by those parameters that describe the pig motion, the solid-fluid interaction, and solid-solid interaction. The effect of these parameters seems beyond the scope of this study.

CONCLUSIONS

This modeling study shows how to use a smart pigging technique (i.e., using a pig with pressure sensors to measure pressure values at the upstream and downstream ends of the pig (P_{upp} and P_{dnp})) for pipeline leak detection. This active leak-detection method demonstrates how to improve traditional passive leak-detection methods that rely only on the pressure and flow rate measurements at the inlet (P_{in} and q_{win}) and outlet (P_{out} and q_{wout}).

The results show that, as a pig travels along the horizontal pipeline moving across the leak location (x_{leak}), the pressure responses (P_{in}, P_{upp}, and P_{dnp}) leave unique signatures. Such information can then be used to determine the major unknowns, such as leak location (x_{leak}) and leak opening size (d_{leak}), at given input parameters such as pig velocity (V_{pig}). A network model concept is used as an efficient tool to interrelate the pressure loss across the pig (ΔP_{pig}), pig velocity (V_{pig}), leaking flowrate (q_{leak}) and pressure at the junction (P_{junc}).

This study based on fluid mechanics and pig dynamics is believed to place a stepping stone towards the proof-of-concept experimental studies to come in the near future, as demonstrated by transient simulations.

REFERENCES

Alaska Department of Environmental Conservation (ADEC). 2012. Pipeline Leak Detection Technology: 2011 Conference Report. Anchorage, Alaska.

API RP 14B. 2005. Design, Installation, Operation, Test, and Redress of Subsurface Safety Valve Systems, fifth edition. Washington, DC: American Petroleum Institute.

API 1130. 2002. Computational Pipeline Monitoring for Liquid Pipelines: Pipeline Segment, second edition (49 CFR 195.444). Washington, DC: American Petroleum Institute.

API TR 1149. 2015. Pipeline Variable Uncertainties and Their Effect on Leak Detectability, second edition. Washington, DC: American Petroleum Institute.

API RP 1175: Pipeline Leak Detection-Program Management. 2015. Washington, DC: American Petroleum Institute.

Azevedo, L. F. A., Braga, A. M. B., Nieckele, A. O., Naccache, M. F., and Gomes, M. G. F. M. 1996. Simple Hydrodynamic Models for the Prediction of Pig Motions in Pipelines. Offshore Technology Conference. Paper No. 8232.

Bai, Y. and Bai, Q. 2005. Subsea Pipelines and Risers. Elsevier. New York, NY.

Bednorz, M., and Pringle, S. 1988. Effect of Measurement Placement on Gas Pipeline Leak Detection. Toronto: Pipeline Simulation Interest Group.

Brill, J. P. and Mukherjee, H. 1999. Multiphase Flow in Wells. SPE Monograph Series Vol. 17. Richardson, TX: SPE.

Burson, W. E., Wade, W. R., and Rachford, Jr., H. H. 1986. Detection of Leaks in Pipeline Networks Using Standard SCADA Information. New Orleans, LA: Pipeline Simulation Interest Group.

Camerini, D. A., von der Weid, J.P., Camerini, C.S., and Maia, C.E. 2004. Leak Detector Pig for Oil Pipelines. International Pipeline Conference. DOI: 10.1115/IPC2004-0095

Chan, Y. S. 1980. PSIG-8002.pdf. In Line Break detection and Testing Method (p. 25). Savannah, GA: Pipeline Simulation Interest Group.

Chatzigeorgiou, D.M., Wu, Y., Youcef-Toumi, K. and Ben-Mansour, R. 2013. Reliable Sensing of Leaks in Pipelines. ASME 2013 Dynamic Systems and Control Conference, DSCC 2013. 2. 10.1115/DSCC2013-4009

Cordell, J. and Vanzant, H. 2003. Pipeline Pigging Handbook (3rd edition). Clarion Technical Publishers and Scientific Surveys Ltd. Houston, TX.

Dupont, T., Rachford, Jr. H. H., McDonald, R.E., Gould, T.L. and Heinze H.J. . 1980. A Transient Remote Integrity Monitor for Pipelines Using Standard SCADA Measurements. Houston, TX: INTERPIPE.

Elliott, J., Fletcher, R., and Wrigglesworth, M. 2008. Seeking the Hidden Threat: Applications of a New Approach in Pipeline Leak Detection. SPE 118070.

Emery, W., Lind, D., Deng, Y., Steele, J., Gu, T., and Wang, H. 2016. Peer Review Report. Department of Transportation. Pipeline & Hazardous Materials Safety Administration. Washington, D.C.

Flournoy, N. E. and Schroeder, W. W. 1978. Development of a Pipeline Leak Detector. Journal of Canadian Petroleum Technology, 17(3), 33–36.

Gajbhiye, R. N., and Kam, S. I. 2008. Leak Detection in Subsea Pipeline: A Mechanistic Modeling Approach with Fixed Pressure Boundaries. SPE Projects, Facilities and Construction. DOI:10.2118/123130-PA.

Geiger, G., Werner, T., and Matko, D. 2003. Leak Detection and Locating - A Survey. Pipeline Simulation Interest Group.

Giddens, P. H. 1938. The Birth of the Oil Industry. The Macmillan Company. Stuttgart, Germany.

Govier, G. W. and Aziz, K. 1972. The Flow of Complex Mixtures in Pipes. Van Nostrand Reinhold Company, New York, NY.

Hara, A., Hayashi, H., Suzuki, O., and Shoji, N. 1978. Calculations Find Sphere Pressure Loss in Lines. Oil & Gas Journal, 7656-58.

Henrie, M., Carpenter, P., and Nicholas, R.E. 2016. Pipeline Leak Detection Handbook. Gulf Professional Publishing. New York, NY.

Kam, S. I. 2009. Mechanistic Modeling of Pipeline Leak Detection at Fixed Inlet Rate. Journal of Petroleum Science and Engineering 70 (3–4):145–156.https://doi.org/10.1016/j.petrol.2009.09.008.

Lima, G., Freitas, V., Araújo, R., Maitelli, A., and Salazar, A. 2017. PIG's Speed Estimated with Pressure Transducers and Hall Effect Sensor: An Industrial Application of Sensors to Validate a Testing Laboratory. Sensors, 17(9), 2119. https://doi.org/10.3390/s17092119

Mastandrea, J.R. 1982. Petroleum Pipeline Leak Detection Study. U.S. Environmental Protection Agency. EPA-600/2-82-040

McDonald, A. E. and Baker, O. 1964. A Method of Calculating Multiphase Flow in Pipe Lines Using Rubber Spheres to Control Liquid Holdup. American Petroleum Institute.

Mirshamsi, M. and Rafeeyan, M. 2012. Speed Control of Pipeline Pig Using the QFT Method. Oil & Gas Science and Technology – Rev. IFP Energies Nouvelles. DOI: 10.2516/ogst/2012008

Pipeline and Hazardous Materials Safety Administration (PHMSA). 2018. Pipeline Facility Incident Report Criteria History. United States Department of Transportation. 24 October 2018.

PIPESIM. 2013. PIPESIM Multiphase Flow Simulator Manual. Schlumberger. Houston, TX.

Parker, C. M. 2004. Pipeline Industry Meets Grief Unimaginable: Congress Reacts with the Pipeline Safety Improvement Act of 2002. Natural Resources Journal **44** (01): 243-282.

Pigging Products and Services Association (PPSA). 1995. An Introduction to Pipeline Pigging. Gulf Professional Publishing. 4 April 1995.

Public Law 103-272. To revise, codify, and enact without substantive change certain general and permanent laws, related to transportation, as subtitles II, III, and V-X of title 49, United States Code, "Transportation", and to make other technical improvements in the Code. 10 June 1994.

Public Law 109-468. Pipeline Inspection, Protection, Enforcement, and Safety Act of 2006. 29 December 2006.

Public Law 112-90. Pipeline Safety, Regulatory Certainty, and Job Creation Act of 2011. 3 January 2012.

Public Law 114-183. Protecting Our Infrastructure of Pipelines and Enhancing Safety Act of 2016. 4 January 2016.

Ramsden, Edward. 2006. Hall-Effect Sensors - Theory and Application (2nd Edition). Elsevier.

Riemsdijk, A. J. Van, and Bosselaar, H. 1967. On-Stream Detection of Small Leaks in Crude Oil Pipelines. 7th World Petroleum Congress. WPC-12525.

Salmatanis, N., Van Reet, J., Dutta-Roy, K., and Shaw, D. 2015. The API 1149 Update, Model-Based Leak Detection Uncertainty Assessment. Pipeline Simulation Interest Group.

Scott, S.L., Lei, L., and Jinghai, Y. 1999. Modeling the Effects of a Deepwater Leak on Behavior of a Multiphase Production Flowline. SPE 52760, DOI:10.2118/52760-MS.

Secor, B. 2018. Leak Detection Mitigation. Pipeline and Hazardous Materials Safety Administration, Research & Development. Department of Transportation. Washington, D.C.

Shannon, R. W. E., Fitzgerald, E. M. N., and Jackson, L. 1985. On-Line Inspection of Offshore Pipelines. Society of Petroleum Engineers. Paper No. 13684.

Shaw, D., Phillips, M., Baker, R., Munoz, E., Rehman, H., Gibson, C., and Mayernik, C. 2012. Final Report: leak Detection Study – DTPH56-11-D-000001. U.S. Department of Transportation Pipeline and Hazardous Materials Safety Administration. Final Report No. 12-173.

Smith, J. R. and Griffin, J. M. 2001. Investigation of Hybrid Deepwater Production. Minerals Management Service.

Stafford, M. and Williams, N. 1996. Pipeline Leak Detection Study. Health and Safety Executive. OTH 94 431.

Thiberville, C. J., Wang, Y., Waltrich, P., Williams, W. C., and Kam, S. I. 2017. Evaluation of Software-based Early Leak Warning System in Gulf-of-Mexico Subsea Flowlines. SPE 187417, DOI:10.2118/187417-MS.

Tiratsoo, J.N.H. (Ed.). 1992. Pipeline Pigging Technology (2nd edition). Gulf Professional Publishing.

Tolmasquim, S.T. and Nieckele, A.O. 2008. Design and Control of Pig Operations through Pipelines. Journal of Petroleum Science and Engineering. https://doi.org/10.1016/j.petrol.2008.07.002

U.S. Department of Transportation, Bureau of Transportation Statistics. 2018. National Transportation Statistics. Washington, D.C.

Wuori, S. J., Hill, R. A., Powell, M. A., and Jones, E. G. 2000. New Trends in Pipeline Technology. World Petroleum Congress.

VITA

Caitlyn Judith Thiberville, raised in New Orleans, Louisiana, worked in and around the oil and gas industry as a field engineer after receiving her bachelor's degree from the University of New Orleans. She became interested in the intricacies and mechanical prowess of the industry while working as a Measurement While Drilling Technician. She decided to further her knowledge of the industry and hone her technical acumen by joining the Craft & Hawkins Department of Petroleum Engineering at Louisiana State University. She plans to receive her Master of Science degree this December 2020, upon completion, she will continue her pursuit to find new challenges.